

1982

# Optical scintillation on folded paths.

Ze'evi, Avihu.

# NAVAL POSTGRADUATE SCHOOL
## Monterey, California


# THESIS

OPTICAL SCINTILLATION ON FOLDED PATHS

by

Avihu Ze'evi

March 1982

Thesis Advisor: E. C. Crittenden

## REPORT DOCUMENTATION PAGE

READ INSTRUCTIONS BEFORE COMPLETING FORM

1. REPORT NUMBER
2. GOVT ACCESSION NO.
3. RECIPIENT'S CATALOG NUMBER

4. TITLE (and Subtitle)
Optical Scintillation on Folded Paths

5. TYPE OF REPORT & PERIOD COVERED
Ph.D. Thesis;
March 1982

6. PERFORMING ORG. REPORT NUMBER

7. AUTHOR(s)
Avihu Ze'evi

8. CONTRACT OR GRANT NUMBER(s)

9. PERFORMING ORGANIZATION NAME AND ADDRESS
Naval Postgraduate School
Monterey, California 93940

10. PROGRAM ELEMENT, PROJECT, TASK AREA & WORK UNIT NUMBERS

11. CONTROLLING OFFICE NAME AND ADDRESS
Naval Postgraduate School
Monterey, California 93940

12. REPORT DATE
March 1982

13. NUMBER OF PAGES
109

14. MONITORING AGENCY NAME & ADDRESS(if different from Controlling Office)

15. SECURITY CLASS. (of this report)
Unclassified

15a. DECLASSIFICATION/DOWNGRADING SCHEDULE

16. DISTRIBUTION STATEMENT (of this Report)
Approved for public release; distribution unlimited.

17. DISTRIBUTION STATEMENT (of the abstract entered in Block 20, if different from Report)

18. SUPPLEMENTARY NOTES

19. KEY WORDS (Continue on reverse side if necessary and identify by block number)
scintillation
folded paths
path integrals

20. ABSTRACT (Continue on reverse side if necessary and identify by block number)

Optical scintillation on folded paths has been investigated for the case of spherical waves and a plane mirror as a folding target. A criterion for the statistical independence of the two parts of the folded path was formulated, utilizing the path integral technique and the Von Karman spectrum. Employing the same approach, an expression for the scintillation strength (the log-intensity variance) on folded paths has been developed.

(20. ABSTRACT Continued)

It has been shown that the scintillation strength on folded paths can be expressed as a product of the one-way scintillation strength and a function of the distance source-detector in units of the outer scale. The analytical prediction shows that the ratio of the log intensity variances on the folded paths to the one on the one-way path, goes from $2^{17/6}$ for exact folding (the distance source-detector is zero), to $2^{11/6}$ when the detector is far away from the source. The theoretical predictions have been corroborated by preliminary field experiments.

Approved for public release; distribution unlimited.

# Optical Scintillation on Folded Paths

by

Avihu Ze'evi
Major, Israel Air Force
B.Sc., The Hebrew University, Jerusalem, Israel, 1967
M.Sc., The Hebrew University, Jerusalem, Israel, 1974

Submitted in partial fulfillment of the
requirements for the degree of

DOCTOR OF PHILOSOPHY

from the

NAVAL POSTGRADUATE SCHOOL

March 1982

## ABSTRACT

Optical scintillation on folded paths has been investigated for the case of spherical waves and a plane mirror as a folding target. A criterion for the statistical independence of the two parts of the folded path was formulated, utilizing the path integral technique and the Von Karman spectrum. Employing the same approach, an expression for the scintillation strength (the log-intensity variance) on folded paths has been developed. It has been shown that the scintillation strength on folded paths can be expressed as a product of the one-way scintillation strength and a function of the distance source-detector in units of the outer scale. The analytical prediction shows that the ratio of the log intensity variances on the folded paths to the one on the one-way path, goes from $2^{17/6}$ for exact folding (the distance source-detector is zero), to $2^{11/6}$ when the detector is far away from the source. The theoretical predictions have been corroborated by preliminary field experiments.

TABLE OF CONTENTS


I. INTRODUCTION ---------- 9

II. BACKGROUND ---------- 11

A. THE SCALAR EQUATION OF PROPAGATION ---------- 11

B. ATMOSPHERIC TURBULENCE ---------- 12

C. ENSEMBLE AVERAGING, STRUCTURE FUNCTION AND TURBULENCE SPECTRUM ---------- 15

D. APPROXIMATE FORMS OF THE SCALAR EQUATION ---- 17

E. PATH INTEGRALS AND THE SOLUTION OF THE PARABOLIC EQUATION ---------- 20

F. SCINTILLATION AND SATURATION ---------- 22

III. STATISTICAL DEPENDENCE OF THE TWO PARTS OF THE FOLDED PATH ---------- 25

A. PREVIOUS WORKS ---------- 25

B. THE EXPRESSION FOR THE PHASE VARIANCE ------- 26

C. THE RELATIONSHIPS BETWEEN THE MEANS OF THE EM FIELD IN VACUUM, THE EM FIELD IN A NON-UNIFORM MEDIUM, AND THE VALUES OF THE PHASE VARIANCES ---------- 28

D. THE VALUE OF $S_{2L}^2$ IN TERMS OF $S_L^2$, FOR THE VON-KARMAN SPECTRUM ---------- 34

E. THE EXPRESSION FOR $S_F^2$ ---------- 37

F. A CRITERION FOR STATISTICAL INDEPENDENCE ---- 46

IV. SCINTILLATION STRENGTH FOR THE FOLDED PATH ------ 49

A. THE RATIO BETWEEN THE SCINTILLATION STRENGTHS FOR THE FOLDED PATH AND THE ONE-WAY PATH ---------- 49

B. DISCUSSION AND OBSERVATIONS ---------- 50

V. EXPERIMENTAL WORK ---------- 59

A. THE EXPERIMENTAL SYSTEM ---------- 59

B. EXPERIMENTAL RESULTS AND DISCUSSION --------- 76

VI. SUMMARY ---------- 81

APPENDIX A: THE SOLUTION OF EQUATION (III-11) -------- 83

APPENDIX B: NUMERICAL EVALUATION OF $f(y_0,\theta)$ ---------- 89

LIST OF REFERENCES ---------- 104

INITIAL DISTRIBUTION LIST ---------- 108

## LIST OF FIGURES


Figure #

1. The reflected (folded path) and the transmitted EM fields at a distance 2L from a point source ---------- 33

2. The geometry and notations of the folded path case ---------- 38

3. The behaviour of $f(y_0,\theta)$ (Eq. III-19) as a function of $y_0$ (for small $\theta$) ---------- 45

4. The ratio between the scintillation strength for the folded path and for the one way path, as a function of $y_0$ ---------- 51

5. The weight functions of spherical waves in the case of a single path and a folded path with $\theta = 0$ ---------- 56

6. The optical system for $\theta \neq 0$ ---------- 60

7. The optical system for $\theta = 0$ ---------- 61

8. The configuration of the optical elements for the measurement of correlation coefficients ---------- 64

9. Correlation between the log-normal intensity variances of the HeNe and the GaAs lasers, which propagate along the same path ---------- 66

10. Correlation between the log-normal intensity variances of two modulated CW HeNe lasers, which propagate along the same path ---------- 67

11. The original configuration of the optical system for the measurements with $\theta = 0$ -------- 70

12. Data reduction system ---------- 73

13. Time sequence of the system's signals --------- 75

14. Correlation between the log-intensity variances of the two series of pulses which originate from the same HeNe laser ------ 77

15. A comparison of the measured $R(y_0)$ values with the analytical prediction ---------- 80

# I. INTRODUCTION

Intensity fluctuations of visible or near-visible sources, while viewed through the atmosphere (scintillation), play a major role in a large variety of situations such as star observations, optical communication channels, Lidars, power transmission, etc. It has been understood for a very long time that the stars' twinkling is caused by the inhomogeneity of the atmospheric index of refraction. It is only in the last thirty years, and especially since the first lasers were built about twenty years ago, that this intuitive understanding has been put into a rigorous quantitative model. Some of the better known contributors to this progress are Tatarski [1,2], Fried [3], Lutomirski and Yura [4], Ishimaru [5], Lee and Harp [6], Clifford [7], Fante [8,9] and Dashen [10]. As a result of their work and many others it is now believed that in most of the situations the processes involved are fairly well understood and the theoretical predictions are reasonably close to experimental findings.

Among the problems which are less understood and for which existing theory either does not give reasonable predictions or has not been confirmed experimentally, is the problem of scintillation on folded paths. In general, this descriptive name stands for a class of situations in which EM fields propagate in the atmosphere from a source to a target and back to a receiver (detector) in the vicinity of or at the

same location of the source. Typical situations which belong to this class are optical radars, communication links (ground-satellite/mirror-ground), remote monitoring of atmospheric pollutants, and others.

The class of point-ahead problems such as pointer-tracker (with fast moving targets), power transmission from space to earth (which follow a beacon signal from earth to space) shares a major question with the previous class, that is to say, the correlation between the two parts of the path.

In this paper we are concerned with scintillation caused by propagation along a folded path when the target is a specular reflector (either a plane mirror or retroreflector). Transition cases in which the two parts of the path are partially correlated are included. To the best of our knowledge, only a small number of works in the open literature address this problem. We will compare the results of these works with ours at the related parts of our paper.

In the second part of this paper (discussion) we describe some accepted formulas, physical pictures and approximations, which describe the atmospheric turbulence and the propagation of EM fields in it. In the third part we develop an expression for the correlation between the two parts of the path. In the fourth we give the expressions for the scintillation strength (the normalized variance of the log-intensity) for a plane mirror and retroreflector targets. The fifth part describes the experimental part of our work (system description and results), and a summary constitutes the sixth part.

## II. BACKGROUND

### A. THE SCALAR EQUATION OF PROPAGATION

The effect of the atmosphere on the EM fields propagation manifests itself through the Maxwell equations. The atmosphere is considered to have no free charges (hence zero conductivity and unit magnetic permeability). It is also assumed, based on experimental findings [8], that the time scale of changes of the atmospheric index of refraction is much longer than the time scale of the EM field fluctuations in the visible and near visible band. This assumption allows us to suppress the time dependent part of the EM field in Maxwell's equations. Based on the above conditions, we find that the vector equation for the EM field propagation is

$$\nabla^2 \underline{E}(\underline{r}) + k^2 n^2(\underline{r}) \underline{E}(\underline{r}) = \underline{\nabla}(\underline{\nabla} \cdot \underline{E}(\underline{r})) \qquad \text{(II-1)}$$

where:

$k = \omega/c$ is the EM field wave number

$n^2(\underline{r}) = \varepsilon(\underline{r})$

$\varepsilon$ = the dielectric constant

$n$ = index of refraction.

It was found analytically [11,12] and confirmed in experiments [13], that the depolarization of EM fields in the

forward direction due to atmospheric turbulence (variations in $n(\underline{r})$) is negligible. Thus the term, on the right hand side of Eq. (II-1) which represents the depolarization (through mixed derivatives) can be neglected [8], and we get the scalar equation of propagation

$$\nabla^2 E(\underline{r}) + k^2 n^2(\underline{r}) E(\underline{r}) = 0 \qquad \text{(II-2)}$$

B. ATMOSPHERIC TURBULENCE

As we can see from Eq. (II-2), the effect of the atmosphere on the EM field propagation is caused by the fluctuations of the index of refraction. The index of refraction is a very complicated function of the atmosphere's constitutents (aerosols, water vapour , etc.), the absorption coefficients [14] (continuous and discrete), the temperature and the pressure. Assuming the absorption is negligible (the wavelength does not match any absorption line or band), the humidity gradient is negligible, and the aerosols' contribution to forward scattering is small, then the index of refraction turns out to be a relatively simple real function of the temperature and the pressure [15]

$$n(\underline{r}) = 1.0 + \frac{77.6}{T(\underline{r})} P(\underline{r}) \left[1 + \frac{.0075}{\lambda^2}\right] \times 10^{-6} \qquad \text{(II -3)}$$

where:

P = total pressure in millibars

$T$ = temperature in degrees Kelvin

$\lambda$ = wavelength in micrometers

Even though the expression for the index of refraction is a simple one, it is impossible to get an exact solution for the scalar equation because we cannot specify the values of the temperature and pressure along the path. The only way we can solve this equation is through the use of their statistical properties.

This approach leads us to express the index of refraction in the following form

$$n(\underline{r}) = n_0 + n_1(\underline{r}) \qquad \text{(II-4)}$$

where $n_0$ is the average value of $n(\underline{r})$ along the path and $n_1(\underline{r})$ is the spatial fluctuation. $n_0$ is found by replacing $P(\underline{r})$, $T(\underline{r})$ in Eq. (II-4) by $P_0$, $T_0$ respectively, and it obviously cannot cause scintillation. In almost all works about the effect of the atmospheric turbulence $n_0$ is taken to be 1.

Since the pressure fluctuations (in the microscale) are relatively small [16], the fluctuations of $n_1(\underline{r})$ are governed by temperature fluctuations.

Due to their small order of magnitude (less than one degree), the main processes through which temperature inhomogeneities in the atmosphere dissipate, are convection on a large scale and molecular dissipation on a very short scale.

Therefore, temperature inhomogeneities (fluctuations in space) which have scale size larger than a certain critical value, are closely related to the velocity field within the atmosphere.

Using this relationship between these fields and the Kolmogorov model of the velocity field, Tatarski [1] gave a statistical description of the index of refraction fluctuations in the atmosphere.

The Kolmogorov [17,18] model is based on the following assumptions:

1. The fluid is incompressible.
2. The fluid is in a steady state.
3. The fluid is getting a constant power per unit mass from an outside source.
4. The Reynolds number of the flow (onset by the outside source) is much greater than the critical Reynolds number of the air.
5. Kinetic energy dissipation into heat can be done only on a very short length scale.

Since the Reynolds number of the original laminar flow is larger than the critical value for air, once the flow is disturbed, it will turn into a turbulent flow with vortices whose length scale is limited only by the dimensions of the flow. This scale is called the outer scale of the turbulence ($L_0$), and in the surface layer it is usually taken to be the height of the point above the ground.

If the Reynolds number of the flow within this vortex is larger than the critical Reynolds number, the vortex will break down into smaller vortices. Since the Reynolds number is proportional to the scale size of the flow, the formation of smaller vortices reduces the local Reynolds number within each vortex until it is smaller than the critical value, and the flow is stabilized. The smallest vortex size is called the "inner scale of the turbulence" ($\ell_0$).

In the literature about EM fields in the atmosphere, these vortices are sometimes called eddies.

## C. ENSEMBLE AVERAGING, STRUCTURE FUNCTION AND TURBULENCE SPECTRUM

The averaging process through which we get the moments of the EM field should be done over many points. Each solution of the scalar equation represents a different $n_1(\underline{r})$ field (the ensemble average). Since the $n_1(\underline{r})$ field has a relatively short correlation length, averaging over the distribution of $n_1(\underline{r})$ along a propagation path can replace the ensemble average. In the literature the ensemble average is denoted by $< >$. We will use the same notation.

Assuming the $n_1(\underline{r})$ field is isotropic and stationary, we can define the following functions.

1. The autocovariance (sometimes called correlation or covariance) function

$$B_n(\underline{r}_1, \underline{r}_2) = \langle n_1(\underline{r}_1) n_1(\underline{r}_2) \rangle \qquad \text{(II-5)}$$

2. The structure function

$$D_n(\underline{r}_1,\underline{r}_2) = \langle [n_1(\underline{r}_1)-n_1(\underline{r}_2)]^2 \rangle \qquad \text{(II-6)}$$

3. The spectrum function $\phi_n(K)$

$$B_n(\underline{r}_1,\underline{r}_2) = \int_{-\infty}^{+\infty}\int\int \phi_n(\underline{K})\, e^{i\underline{K}(\underline{r}_1-\underline{r}_2)}\, d\underline{K}$$

Since we assumed isotropic turbulence, the last equation can be written as

$$B_n(\rho) = 4\pi \int_0^{\infty} \phi_n(K)\, \frac{\text{Sin}\,(K\rho)}{K\rho}\, K^2\, dK \qquad \text{(II-7)}$$

In the last four equations:

$\underline{r}_1$ = spatial vectors

$\rho = |\underline{r}_1 - \underline{r}_2|$

$\underline{K}$ = spatial frequency vector (of the $n_1(\underline{r})$ field)

$K = |\underline{K}|$

Using the Kolmogorov model, the spectrum function is given by

$$\phi_n(K) = .033C_n^2K^{-11/3} \quad \text{for} \quad 2\pi/L_0 < K < 2\pi/\ell_0 \qquad \text{(II-8)}$$

This interval is called the inertial range. $C_n^2$ represents the strength of the turbulence and it is proportional to the variance of $n_1$ at a point $\underline{r}_1$.

In most early works, this spectrum was used (by way of approximation) in the range $0 \leq K \leq \infty$. This procedure as pointed out by Yura [19], can cause serious deviation in the outcome of some calculations. Thus a somewhat different spectrum is now being used, namely the modified Von Karman spectrum.

$$\phi_n(K) = \frac{.033C_n^2 \, e^{-(K\ell_0)^2}}{(K^2 + L_0^{-2})^{11/6}} \qquad \text{(II-9)}$$

Hill and Clifford [20] showed that a high K values, the $\phi_n(K)$ is not a decreasing function, but rather it increases to a local maximum and then goes to zero as the modified Von Karman spectrum.

## D. APPROXIMATE FORMS OF THE SCALAR EQUATION

The most commonly used approximations for the scalar equation are the Rytov (small or smooth perturbation) approximation, and the parabolic equation approximation.

The Rytov approximation is based on the perturbation theory and has one basic assumption:

$$|\nabla \ln E_1| \ll |\nabla \ln E_0| \qquad \text{(II-10)}$$

This restriction is equivalent to the assumption that the beam can be scattered by turbulence eddies only once, which means that it restricts the range of applicability of this approximation to weak turbulence levels.

Starting with the scalar wave equation, and replacing n by $1+n_1$, and E by exp(T), we get

$$\nabla^2 T + (\nabla T)^2 + k^2(1+n_1)^2 = 0$$

Taking $T = T_0 + T_1$ and $n_1^2 << 2n_1$, we get

$$\nabla^2 T_0 + (\nabla T_0)^2 + k^2 + \nabla^2 T_1 + (\nabla T_1)^2 + 2(\nabla T_0)(\nabla T_1) + 2k^2 n_1 = 0$$

We can see that condition (II-10) is equivalent to

$$|\nabla T_1| << |\nabla T_0|$$

and that if $e^{T_0} = E_0$ is the vacuum solution of the scalar equation, the last equation can be written as

$$\nabla^2 T_1 + 2\nabla T_0 \cdot \nabla T_1 + 2k^2 n_1 = 0 \qquad \text{(II-11)}$$

which can be solved ($\nabla T_0$ is known), for the moments of $T_1$.

Experimentally it was found [7] that the Rytov approximation is valid as long as

$$\sigma_x^2 = .124\, k^{7/6} L^{11/6} C_n^2 < .3 \qquad \text{(II-12)}$$

where:

$k$ = wave number,

$L$ = distance of propagation, and

$C_n^2$ = the turbulence strength.

The Markov approximation is based on the assumption that (for an EM field which propagates along the x axis)

$$\left|\frac{\partial^2 u}{\partial x^2}\right| \ll \left|2ik\,\frac{\partial u}{\partial x}\right| \qquad \text{(II-13)}$$

where

$$u = u(x,y,z) = \frac{E(x,y,z)}{\exp(ikx)} \qquad \text{(II-14)}$$

As Tatarski showed [2], the condition (II-13) is equivalent to the condition $1 \ll k\ell_0$ which is almost always met in the atmosphere ($\ell_0 \sim 1$mm) for the visible band.

Inserting (II-14) in the scalar equation and using condition (II-13) gives the following equation, which is called the parabolic equation

$$2ik\,\frac{\partial}{\partial x}u(x,\underline{r}_0) + \nabla^2_{r_0}\,u(x,\underline{r}_0) + 2k^2 n_1(x,\underline{r}_0)u(x,\underline{r}_0) = 0 \qquad \text{(II-15)}$$

where $\underline{r}_0$ is a vector in the y,z plane.

The physical meaning of condition (II-13) is that the scattering due to the eddies, is primarily in the forward

direction [8]. Eq. (II-15) can be solved by using the Markov approximation [2] or by path integral. Dashen, who was the first to show that the parabolic equation could be solved by the path integral technique, argues [10] that the constraints imposed on the solution of the parabolic equation by both techniques are the same, and identical to the one imposed by the parabolic equation.

## E. PATH INTEGRALS AND THE SOLUTION OF THE PARABOLIC EQUATION

In the forties, the path integral technique was developed R.F. Feynman in an effort to use the principle of least action as the basic principle of Quantum Mechanics. A good description of the technique and its application in Quantum Mechanics and a few other fields of physics can be found in a textbook by Feynman and Hibbs [21]. The use of the technique in solving the parabolic equation is described in a report by D.L. Palmer [22].

The use of the path integral technique in solving differential equations can be demonstrated by the following example (free particle in a one dimension motion).

Applying the Shrodinger equation to this case gives us

$$-i\hbar \frac{\partial \psi}{\partial t} = \frac{\hbar^2}{2m} \frac{\partial^2 \psi}{\partial x^2} \quad (+ \text{ boundary conditions}) \qquad \text{(II-16)}$$

where $\psi$ is the probability amplitude function.

We know that for a free particle in a one dimension motion,

$$L = \frac{m\dot{x}^2}{2}$$

and the action integral is given by

$$S = \int_{t_a}^{t_b} L \, dt \qquad \text{(II-17)}$$

Starting from Feynman's basic assumption, namely that the probability amplitude assigned to the ith path (connecting points a,b) is

$$\psi_i(a,b) = \int_a^b \exp[is(a,b)/\hbar] d\ell_i$$

where the integral is being carried out along the ith path.

Since the total probability amplitude is the sum of the contributions from all possible paths, it is given by

$$\psi(a,b) = \int D \text{ (paths) } \exp[is(a,b)/\hbar] \qquad \text{(II-18)}$$

Comparing Eqs. (II-16) and (II-18), we can see that the solution of the differential equation (II-16) can be found by the use of the path integral technique, providing we can come up with the kernel of the differential equation, which in our example was obvious.

In the case of the parabolic equation, the procedure is more elaborate, and since this is not the main topic of our

work, we would rather merely quote the result in Section (III.C) of this work.

## F. SCINTILLATION AND SATURATION

Viewing a source of constant output through the atmosphere, we see that the intensity varies with time (scintillates), just as in the case of stars twinkling.

Usually the scintillation strength is measured by the variance of the normalized intensity

$$\sigma_I^2 = \langle (I/I_0)^2 \rangle - \langle I/I_0 \rangle^2 = \frac{\langle I^2 \rangle}{\langle I \rangle^2} - 1 \qquad \text{(II-19)}$$

where:

$$I_0 = \langle I \rangle .$$

Since it was found that in weak turbulence, the log amplitude of the EM field is a random variable with normal distribution [2], the log of the normalized intensity is distributed normally in this region. Hence it is useful to work with the variable $\ell = \ln(I/I_0)$ and to define the turbulence strength by

$$\sigma_\ell^2 = \langle \ell^2 \rangle - \langle \ell \rangle^2 \qquad \text{(II-20)}$$

Defining $\Delta I = I - I_0$, we can see that if $\Delta I << I_0$, since $\langle \Delta I \rangle = 0$, then

$$\ell = \ln(I/I_0) = \ln[(\Delta I + I_0)/I_0]$$

$$= \ln(1 + \frac{\Delta I}{I_0}) \cong \Delta I/I_0$$

Thus Eq. (II-20) can be written as

$$\sigma_I^2 = \langle(\Delta I/I_0)^2\rangle - \langle\Delta I/I_0\rangle^2 = \frac{\langle\Delta I^2\rangle}{I_0^2} \qquad \text{(II-21)}$$

There are several models by which the scintillation can be explained. The simplest model which was originally used by Tatarski [1], describes the eddies in the atmosphere as spherical lenses whose index of refraction differs from their surroundings by $\Delta n = n_1$. These lenses focus or defocus (depending on the $n_1$ values) the rays onto the target plane.

It was believed that this picture gives good approximation only in the weak turbulence region (not more than one scattering event), until Yura [23] showed that it can be applied to the strong turbulence region also, if we incorporate in this picture the notion of the transverse coherence length ($r_0$) and its effect on the focusing ability of the eddies. Due to focusing and defocusing of the beam while propagating through the atmosphere, the transverse coherence length of it is gradually reduced and therefore, the ability of the eddies to focus the beam further, is reduced too. Hence the growth of the scintillation strength is saturated and it should reach a maximum.

Other models which are used, either in detailed calculations or in qualitative explanations, are the phase screen model [6] and the scattering model [24]. The first describes the effect of the atmosphere on the beam as a distortion of the phase front due to different optical paths in the turbulence. In turn, the distorted phase front will produce an interference pattern in the target plane. The second views the EM fields at the target plane as the sum of fields which were scattered at small angles by off-axis eddies and the direct (unscattered) field.

Since in all models, the scintillation strength depends on the turbulence strength (density and effectiveness of the eddies) and the total number of focusing or scattering events along the propagation path, it is found very frequently in the literature that the integrated turbulence strength (the effective turbulence strength) is given by the Rytov parameter which was defined in Eq. (II-12). Sometimes it is denoted by $\beta$ or $\sigma_T$.

It was found experimentally [7] that in the weak turbulence region (also called the Rytov region), in which the intensity distribution is log normal, $\sigma_x^2$ goes up to 0.3. As $\sigma_x^2$ grows beyond this value, the intensity distribution is close to the K distribution [25], the scintillation strength reaches a maximum [26] and starts to decrease. As $\sigma_x^2$ grows further, the intensity distribution is best described by the exponential distribution [10,27] and normalized intensity variance approaches 1.

## III. STATISTICAL DEPENDENCE OF THE TWO PARTS OF THE FOLDED PATH

### A. PREVIOUS WORKS

As we mentioned in the first chapter of this work, the question of whether the two parts of the folded path are statistically independent, is a basic one when we try to describe the statistical behaviour of the EM field which propagates along it. Once we can assume statistical independence, we can treat the two parts separately, applying the well known results for the one-way propagation to each of them. Since our main object is the scintillation along a folded path, with a special emphasis on short distances between the source and the detector, the first subject of our analysis is to try to define a criterion for the statistical dependence between the two parts.

Among the works that we were able to find in the literature, which analyze the folded path question, some like the theoretical work by Yura [28] and the experimental work by Ben-Simon et al., [29], assume statistical independence of the two parts. Yura gives the condition for independence as

$$d > D_s, D_d$$

where d is the distance source-detector and $D_s$, $D_d$ are the aperture diameters of the source and the detector respectively. Since in Yura's paper the target is diffusive (volume of

air molecules) and the reflected beam is totally incoherent, we cannot apply this result to our case (specular target).

In other works [30,31,32] the question of the independence of the two parts is related to the wavefront tilt or angle of arrival (AOA) fluctuations which depends on the large scale eddies. Since we are concerned with scintillation which is caused primarily by the small scale eddies, we cannot use their results.

Before we continue our analysis, we would like to mention without going into detailed explanation, that the usual criterion for independence between two diverging paths (their end points should be separated by a few isoplanatic patches), cannot be applied in our case, due to the fact that in a folded path case certain parts of it (near the target) might be very close and certainly correlated to some degree. As we will see later, this correlation affects the scintillation and we cannot ignore it.

## B. THE EXPRESSION FOR THE PHASE VARIANCE

We start our analysis with the effect of the atmospheric turbulence on the phase of the propagating EM field.

The phase fluctuations (S) relative to the vacuum value, due to the non-uniform medium, are given by the integral along the optical path.

$$S = k \int_0^L n_1(x)\,dx \qquad \text{(III-1)}$$

Since $\langle n_1(x) \rangle = 0$

$$\langle S \rangle = \langle k \int_0^L n_1(x)\,dx \rangle = k \int_0^L \langle n_1(x) \rangle dx = 0$$

The variance of the phase fluctuation is

$$\sigma_S^2 = \langle S^2 \rangle - \langle S \rangle^2 = \langle S^2 \rangle$$

and

$$\langle S^2 \rangle = \langle (k \int_0^L n_1(x)\,dx)(k \int_0^L n_1(x')\,dx') \rangle$$

$$= k^2 \int_0^L dx \int_0^L dx' \langle n_1(x) n_1(x') \rangle$$

$$\langle S^2 \rangle = k^2 \int_0^L dx \int_0^L dx' B_n(x,x') \qquad \text{(III-2)}$$

Since in the Kolmogorov model, $B_n(x,x') = B_n(y)$ where $y = |x - x'|$ and it is the same function regardless of the origin of y, $\langle S^2 \rangle$ can be approximated by

$$\langle S^2 \rangle = k^2 L \int_{-L/2}^{L/2} B_n(y)\,dy \qquad \text{(III-3)}$$

provided $L >> \bar{y}$ where $\bar{y}$ is the range at which $B_n(\bar{y}) << B_n(0)$.

As we can see from Eq. (III-2), the variance of the phase is related directly to the field of the index of refraction. This is the reason we chose to utilize the phase variance in the criterion for statistical dependence/independence between the two parts of the folded path.

In this part of the work we chose to work with an infinite plane mirror as a folding target for two reasons:

1. It is easy to compare the case of a folded path (with a plane mirror) when the angle between the two parts of the path is $2\theta$, to the case of a straight path ($2\theta = \pi$) (see Fig. 1). There is no discontinuity of the rays and there are no singular points at the target, as in the case of the corner cube.
2. When an infinite, or at least very large mirror is used, we do not have to take into account the possibility that part of the beam will not be reflected. Thus at this stage, we can neglect the effect of beam wander.

## C. THE RELATIONSHIPS BETWEEN THE MEANS OF THE EM FIELD IN VACUUM, THE EM FIELD IN A NON-UNIFORM MEDIUM, AND VALUES OF THE PHASE VARIANCES

Following Dashen [10], we can write an expression for $\varepsilon$ (where $E = \mathrm{Re}(\varepsilon)$ at a point $(L,\underline{r})$ due to a point source at $(0,\underline{r}_0)$. This analytical signal is the solution of the parabolic equation [22] and it is given by

$$\varepsilon(0,\underline{r}_0,L,\underline{r}) = \frac{i}{2k}\int D(\text{paths})$$

$$\times \exp\{ik\int_0^L [\tfrac{1}{2}(\underline{r}'(x))^2 - n_1(\underline{r}+\underline{e}_x x)]dx\} \quad \text{(III-4)}$$

where:

$$\underline{r}'(x) = \frac{d\underline{r}(x)}{dx}$$

$\underline{e}_x$ = unit vector along x axis.

From Eq. (III-4) we can get the expression for the analytical signal of the vacuum field by setting $n_1 = 0$. Thus we get

$$\varepsilon^0(0,\underline{r}_0,L,\underline{r}) = \frac{i}{2k}\int D(\text{paths})$$

$$\times \exp\{\frac{ik}{2}\int_0^L [\underline{r}'(x)]^2 dx\} \quad \text{(III-5)}$$

Taking the ensemble average of Eq. (III-4) we get

$$\langle\varepsilon\rangle = \langle\frac{i}{2k}\int D(\text{paths})\rangle \quad \text{(III-6)}$$

$$\times \exp\{\frac{ik}{2}\int_0^L [\underline{r}'(x)]^2 dx - ik\int_0^L n_1[\underline{r}(x)+\underline{e}_x x]dx\}$$

$$= \frac{i}{2k}\int D(\text{paths}) \times \exp\{\frac{ik}{2}\int_0^L [\underline{r}'(x)]^2 dx\}$$

$$\times \langle\exp\{ik\int_0^L n_1(\underline{r}(x)+\underline{e}_x x)dx\}\rangle$$

Using Eq. (III-1) we can write

$$\langle \exp\{ik \int_0^L n_1(\underline{r}(x)+\underline{e}_x x)\,dx\}\rangle = \langle \exp(S_1^P)\rangle$$

where $S_1^P = iS^P$ and $S^P$ is the phase fluctuation along the path P. Since it is generally accepted [33,34] that the phase fluctuation in the atmosphere is a Gaussian random variable with zero mean, $S_1^P$ is also Gaussian with zero mean, and therefore it satisfies the following formula(*)

$$\langle e^{S_1^P}\rangle = \exp[\frac{\langle (S_1^P)^2\rangle}{2}]$$

Thus

---

(*) For Gaussian random variable $\alpha$, with zero mean and with standard deviation $\sigma$

$$\langle e^{\alpha}\rangle = \int_{-\infty}^{\infty} e^{\alpha} f(\alpha,0)\,d\alpha = \frac{1}{\sqrt{2\pi}\sigma} \int_{-\infty}^{\infty} e^{\alpha} \exp[-\frac{\alpha^2}{2\sigma^2}]\,d\alpha$$

$$= \frac{1}{\sqrt{2\pi}\sigma} \int_{-\infty}^{\infty} \exp[\frac{2\alpha\sigma^2-\alpha^2}{2\sigma^2}]\,d\alpha = \frac{\exp(\sigma^2/2)}{\sqrt{2\pi}\sigma} \int_{-\infty}^{\infty} \exp[-\frac{(\alpha-\sigma^2)^2}{2\sigma^2}]\,d\alpha$$

$$= \exp[\sigma^2/2] \int_{-\infty}^{\infty} f(\alpha,\sigma^2)\,d\alpha = \exp[\sigma^2/2]$$

where $f(\alpha,x)$ is the normal distribution function for mean = x.

$$\langle e^{iS^P} \rangle = \exp\left[-\frac{\langle (S^P)^2 \rangle}{2}\right]$$

Using Eq. (III-2) we get

$$\langle \exp\{ik \int_0^L n_1(\underline{r}(x)+\underline{e}_x x)\,dx\} \rangle \qquad \text{(III-7)}$$

$$= \exp\{-\frac{k^2}{2} \int_0^L \int_0^L B_n[[(\underline{r}(x)-\underline{r}(x')^2+(x-x')^2]^{1/2}]\,dx\,dx'\}$$

Assuming that the optical paths in our case, which are the main contributors to the path integral, satisfy

$$|\underline{r}(x) - \underline{r}(x')| \ll |x - x'| \qquad \text{(III-8)}$$

Eq. (III-7) can be approximated by

$$\langle \exp\{ik \int_0^L n_1(\underline{r}(x)+\underline{e}_x x)\,dx\} \rangle \qquad \text{(III-9)}$$

$$= \exp\{-\frac{k^2}{2} \int_0^L \int_0^L B_n(x,x')\,dx\,dx'\}$$

Inserting Eqs. (III-5), (III-9), (III-2) in Eq. (III-6), we get

$$\langle \varepsilon(0,\underline{r}_0,L,\underline{r}) \rangle = \varepsilon^0(0,\underline{r}_0,L,\underline{r}) \exp\left[-\frac{\langle S_L^2 \rangle}{2}\right] \qquad \text{(III-10)}$$

where $\langle S_L^2 \rangle$ is the variance of the phase fluctuations, due to propagation along a path of length L.

From Eq. (III-10) we see that the effect of the turbulent atmosphere on the average of a propagating EM field, can be expressed by the variance of the phase fluctuations along the geometrical path.

It is obvious that in vacuum, apart from a phase shift due to the reflection, the fields $E_F$ and $E_{2L}$ as described in Fig. 1, are the same. We can ask ourselves what will be the relationship between $\langle \varepsilon_F \rangle$ and $\langle \varepsilon_{2L} \rangle$? Since in the case of $\langle \varepsilon_{2L} \rangle$ there is no folding at all, it is obvious that in this case there is no statistical dependence (relating to the folding). Hence, the closer $\langle \varepsilon_F \rangle$ to $\langle \varepsilon_{2L} \rangle$, the less dependence (statistical correlation between the two parts), we have.

Using Eq. (III-10) and the observation that up to a phase constant $\varepsilon_F^0 = \varepsilon_{2L}^0$, we come to the conclusion that the statistical dependence between the two parts of the folded path, can be determined by the relationship between $\langle S_F^2 \rangle$ and $\langle S_{2L}^2 \rangle$; the closer their values are, the less the two parts of the folded path are correlated. Therefore, in the next steps we will calculate $S_{2L}^2$ and $S_F^2$ (we omitted the angular brackets for the sake of convenience), compare their values, and formulate a criterion for statistical independence.

Before we go to the next step of the analysis, we have to evaluate the effect of the constraint which was formulated in Eq. (III-8), on the applicability of our approach.

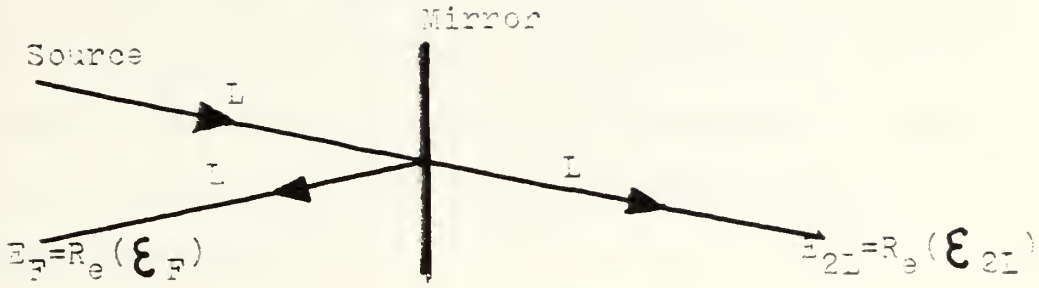


Figure 1. The reflected (folded path) and transmitted EM fields at distance 2L from a point source.

Since the point $(x,\underline{r}(x))$ is a point on the optical path through the turbulent medium (which is given by the normals to the wavefronts), the constraint (III-8) is equivalent to

$$\left|\frac{d\underline{r}(x)}{dx}\right| \ll 1$$

which means that the normals to the wavefronts are almost parallel to the x axis, which in turn means that only small angles of scattering are allowed. This constraint is the same as the one for the utilization of the parabolic equation [8,10] (Eq. (II-13)), and both are met for almost all conceivable conditions.

## D. THE VALUE OF $S_{2L}^2$ IN TERMS OF $S_L^2$, FOR THE VON KARMAN SPECTRUM

From Eq. (III-2) we can write

$$S_L^2 = k^2 \int_0^L dx \int_0^{L'} dx' \, B_n(|x - x'|)$$

and

$$S_{2L}^2 = k^2 \int_0^{2L} dx \int_0^{2L} dx' \, B_n(|x - x'|)$$

Working on both integrals and using the transformation

$$z = x - x' \qquad \frac{y + z}{2} = x$$

$$y = x + x' \qquad \frac{y - z}{2} = x'$$

$$J\left(\frac{x, x'}{y, z}\right) = \frac{1}{2}$$

$$S^2_{L_i} = \frac{k^2}{2}\left\{ \int_0^{L_i} dz \int_z^{2L_i - z} B_n(|z|)\,dy + \int_{L_i}^{0} dz \int_{-z}^{2L_i + z} B_n(|z|)\,dy \right\}$$

$$= \frac{k^2}{2}\left\{ \int_0^{L_i} dz\, B_n(|z|)(2L_i - 2z) + \int_{-L_i}^{0} dz\, B_n(|z|)(2L_i + 2z) \right.$$

where $L_i$ is either L or 2L.

Taking $z \to -z$ in the second term, we get

$$S^2_{L_i} = 2k^2 \int_0^{L_i} (L_i - z) B_n(z)\,dz$$

Inserting the explicit forms of $B_n(x)$ [2] and the Von Karman spectrum for $\phi_n(K)$

$$B_n(x) = 4\pi \int_0^{\infty} \phi_n(K, x)\, \frac{\mathrm{Sin}(Kx)}{Kx}\, K^2 dK$$

$$\phi_n(K, x) = \frac{.033\, C_n^2(x)}{(K^2 + L_0^{-2})^{11/6}}$$

Assuming $C_n^2(x)$ = constant and taking $y = KL_0$, we get

$$S^2_{L_i} = A \int_0^{L_i/L_0} dz \, \frac{(L_i/L_0 - z)}{z} \int_0^{\infty} \frac{dy \; y \; \mathrm{Sin}(zy)}{(y^2+1)^{11/6}}$$

where:

$$A = .033 \; 2^3 \; \pi \; k^2 \; C_n^2 \; L_0^{8/3}$$

and $z = x/L_0$.

Using formula 2.3(11) of Ref. [35] we get

$$S^2_{L_i} = A_1 \int_0^{L_i/L_0} dz (L_i/L_0 - z) z^{1/3} K_{1/3}(z)$$

where:

$$A_1 = .033 \; 2^{5/3} \; \pi^{3/2} \; k^2 \; C_n^2 \; L_0^{8/3} / \Gamma(11/6)$$

and $K_{1/3}(z)$ = Modified Bessel function of the third kind.

Solving the integral in Eq. (III-11) (detailed solution is given in Appendix A), gives for $(L_i/L_0) >> 1$

$$S^2_{L_i} = \frac{A_1 \pi^{1/2} \Gamma(5/6)}{2^{2/3}} (L_i/L_0) \qquad \text{(III-12)}$$

which is the same as the expression which is given by Tatarski [2]. Thus we can see that for large $(L_i/L_0)$, $S^2_{L_i}$ is approximately linear in $L_i$ and

$$S_{2L}^2 = 2S_L^2 \qquad \text{(III-13)}$$

## E. THE EXPRESSION FOR $S_F^2$

The geometry of the folded path and the notations which we use in this section are described in Figure 2. We assume that the mirror is large enough so that:

1. Diffraction effects can be neglected.
2. There are no fluctuations in the amount of energy being intercepted by it.

We also assume that the field at the point D ($E_F$) can be found by the path integral technique, using SMD as the geometrical optics path. It should be pointed out that since the calculation of the $E_F$ value by the path integral assumes

$$\left|\frac{d\underline{r}\ (x)}{dx}\right| \ll 1 \qquad \text{(scattering at small angles)}$$

the application of the technique to this type of path might be questionable, for the reason that it includes one point (M) at which the above condition is certainly not satisfied.

Our justification for the use of the path integral technique along this type of path, is based upon two arguments;

1. In the case of fields propagating in vacuum, we know that apart from a phase constant, $E_D = E_{2L}$. Therefore, we can use the path integral technique (Eq. (III-5)) along the path SMD by excluding the point M from the integration.

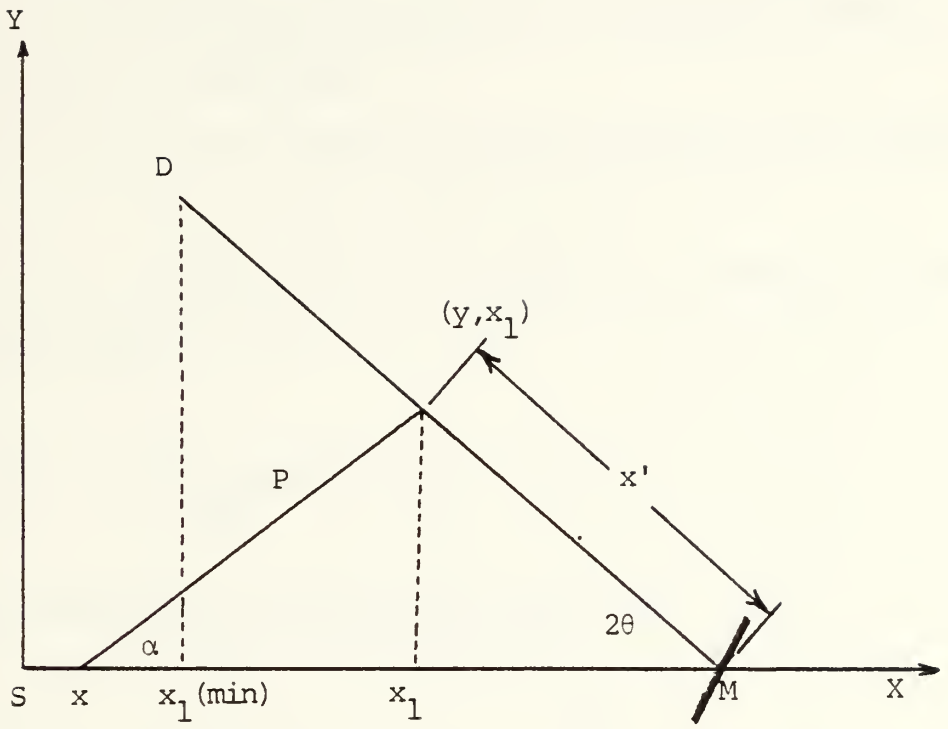


Figure 2. The geometry and notations of the folded path case. M = a plane mirror; S = a point source; D = detector. The distances SM and DM are of length L.

2. If the results of our analysis in the two extreme cases;

   a. $\theta = 0$

   b. $\theta \to \pi/4$

   match the results which are obtained in other ways, the fact that at the point M, $\frac{dr(x)}{dx}$ is infinite, has no effect on the applicability of the path integral technique to our case.

At the end of this section we will discuss the second argument.

As we saw in Section III.C, in order to find $E_F$ we have to calculate $S_F^2$ by

$$S_F^2 = k^2 \iint_{SMD} dxdx' \, B_n(|x - x'|)$$

where the integration is along the line SMD. Thus

$$S_F^2 = k^2 \int_0^L dxdx' \, B_n(|x - x'|) + k^2 \int_L^{2L} dxdx' \, B_n(|x - x'|)$$

$$+ k^2 \int_0^L dx \int_L^{2L} dx' \, B_n(|x - x'|) + k^2 \int_L^{2L} dx$$

$$\times \int_0^L dx' \, B_n(|x - x'|)$$

$$= I_1 + I_2 + I_3 + I_4$$

where integration on the interval 0,L means integration along SM, and on the interval L,2L means integration along MD.

In integrals $I_3$ and $I_4$, x' is the distance of the point $(y,x_1)$ from the point M along the line MD, and the notation $|x - x'|$ stands for the actual distance between the points, which is denoted by P.

Using the transformation y = x-L; y' = x'-L

$$I_2 = k^2 \int_0^L \int dydy' \, B_n(|y - y'|) = I_1$$

Since $B_n(|x - x'|)$ is symmetric in x, x', $I_3 = I_4$, and therefore

$$S_F^2/2 = k^2 \int_0^L \int dxdx' \, B_n(|x - x'|) \qquad \cdot(III-14)$$

$$+ k^2 \int_0^L dx \int_L^{2L} dx' \, B_n(|x - x'|) = I_1 + I_3$$

From Eq. (III-2)

$$I_1 = S_L^2$$

The evaluation of $I_3$

From Fig. 2 we can see that

$$x' = (L-x_1)/\mathrm{Cos}(2\theta); \quad dx' = -dx_1/\mathrm{Cos}(2\theta)$$

(III-16)

$$y = (L-x_1)\mathrm{Tan}(2\theta)$$

$$|x-x'| = P = [(L-x_1)^2\mathrm{Tan}^2(2\theta) + (x_1-x)^2]^{1/2} \qquad \text{(III-17)}$$

Hence $I_3$ can be written as

$$I_3 = \frac{k^2}{\mathrm{Cos}(2\theta)} \int_0^{2L\,\mathrm{Sin}^2\theta} dx \int_x^L dx_1\, B_n(P(x,x_1))$$

Applying the transformation $(x,x_1) \rightarrow (P,\alpha)$ and observing that

1. $x = L - \dfrac{P\,\mathrm{Sin}(2\theta+\alpha)}{\mathrm{Sin}(2\theta)}$

2. $x_1 = L - P\,\mathrm{Sin}\,\alpha\,\mathrm{Cot}(2\theta)$

3. $J\left(\dfrac{x,x_1}{P,\alpha}\right) = \begin{vmatrix} \dfrac{\partial x}{\partial P} & \dfrac{\partial x}{\partial \alpha} \\ \dfrac{\partial x_1}{\partial P} & \dfrac{\partial x_1}{\partial \alpha} \end{vmatrix} = P\,\mathrm{Cot}(2\theta)$

4. For $0 \leq \alpha \leq \pi/2 - \theta$

$$0 \leq P \leq \frac{L\,\mathrm{Sin}(2\theta)}{\mathrm{Sin}(2\theta+\alpha)} = P_1$$

5. For $\pi/2-\theta \leq \alpha \leq \pi-2\theta$

$$0 \leq P \leq \frac{L\,\mathrm{Sin}(2\theta)}{\mathrm{Sin}\,\alpha} = P_2$$

we get

$$I_3 = \frac{k^2}{\mathrm{Sin}(2\theta)}\{\int_0^{\pi/2-\theta} d\alpha \int_0^{P_1} PB_n(P)\,dP$$

$$+ \int_{\pi/2-\theta}^{\pi-2\theta} d\alpha \int_0^{P_2} PB_n(P)\,dP\}$$

Making the transformation $\beta = \pi-(2\theta+\alpha)$ in the second integral, we can see that it is equal to the first one. Thus

$$I_3 = \frac{2k^2}{\mathrm{Sin}(2\theta)} \int_0^{\pi/2-\theta} d\alpha \int_0^{P_1} PB_n(P)\,dP$$

where

$$P_1 = \frac{L\ \mathrm{Sin}(2\theta)}{\mathrm{Sin}(2\theta+\alpha)}$$

Inserting the explicit forms of $B_n(P)$ and the Von Karman $\phi_n(K)$, and assuming that $\phi_n(K,x) = \phi_n(K)$, we get

$$I_3 = A \int_0^{\pi/2-\theta} d\alpha \int_0^{y_1} dy \int_0^{\infty} dz\ z(z^2+1)^{-11/6}\mathrm{Sin}(yz)$$

where:

$$A = \frac{.033\ 8\pi\ k^2\ C_n^2\ L_0^{8/3}}{\mathrm{Sin}(2\theta)}$$

$$z = L_0 K \qquad y = P/L_0$$

$$y_1 = \frac{L \sin(2\theta)}{L_0 \sin(2\theta+\alpha)}$$

Using formula 2.3(11) of Ref. [35], we get

$$I_3 = A_1 \int_0^{\pi/2-\theta} d\alpha \int_0^{y_1} dy\, y^{4/3} K_{1/3}(y)$$

where:

$$A_1 = \frac{.033\ 2^{5/3}\ \pi^{3/2}\ k^2\ C_n^2\ L_0^{8/3}}{\sin(2\theta)\ \Gamma(11/6)}$$

$K$ = Modified Bessel function of the third kind

$\Gamma$ = the gamma function

Comparing the last equation with Eq. (III-12) gives

$$I_3 = \frac{2^{2/3}\ L_0}{\sin(2\theta)\pi^{1/2}\Gamma(5/6)L}\ S_L^2 \int_0^{\pi/2-\theta} d\alpha \int_0^{y_1} dy\, y^{4/3} K_{1/3}(y)$$

Inserting the last equation and Eq. (III-15) into Eq. (III-14) gives

$$S_F^2 = 2S_L^2[1 + f(y_0,\theta)]$$

or by using (III-13)

$$S_F^2 = S_{2L}^2[1 + f(y_0,\theta)] \qquad \text{(III-18)}$$

where

$$f(y_0,\theta) = \frac{A_2}{y_0} \int_0^{\pi/2-\theta} d\alpha \int_0^{y_1} y^{4/3} K_{1/3}(y)\,dy \qquad \text{(III-19)}$$

and

$$A_2 = \frac{2^{2/3}}{\pi^{1/2}\Gamma(5/6)}$$

$$y_0 = \frac{L\ \mathrm{Sin}(2\theta)}{L_0}$$

$$y_1 = y_0/\mathrm{Sin}(2\theta+\alpha)$$

We solved Eq. (III-19) numerically and found out that for small angles $\theta$, which is the case in most of the applications, the f dependence on $\theta$ is very weak, and therefore $f(y_0,\theta) \cong f(y_0)$.

The result of the numerical integration is described in Figure 3, and we can see that

$$\lim_{y_0 \to 0} f(y_0,\theta) = 1 \qquad (\text{when } \theta \to 0,\ y_0 \to 0)$$

$$\lim_{\theta \to \pi/4} f(y_0,\theta) = 0$$

and therefore

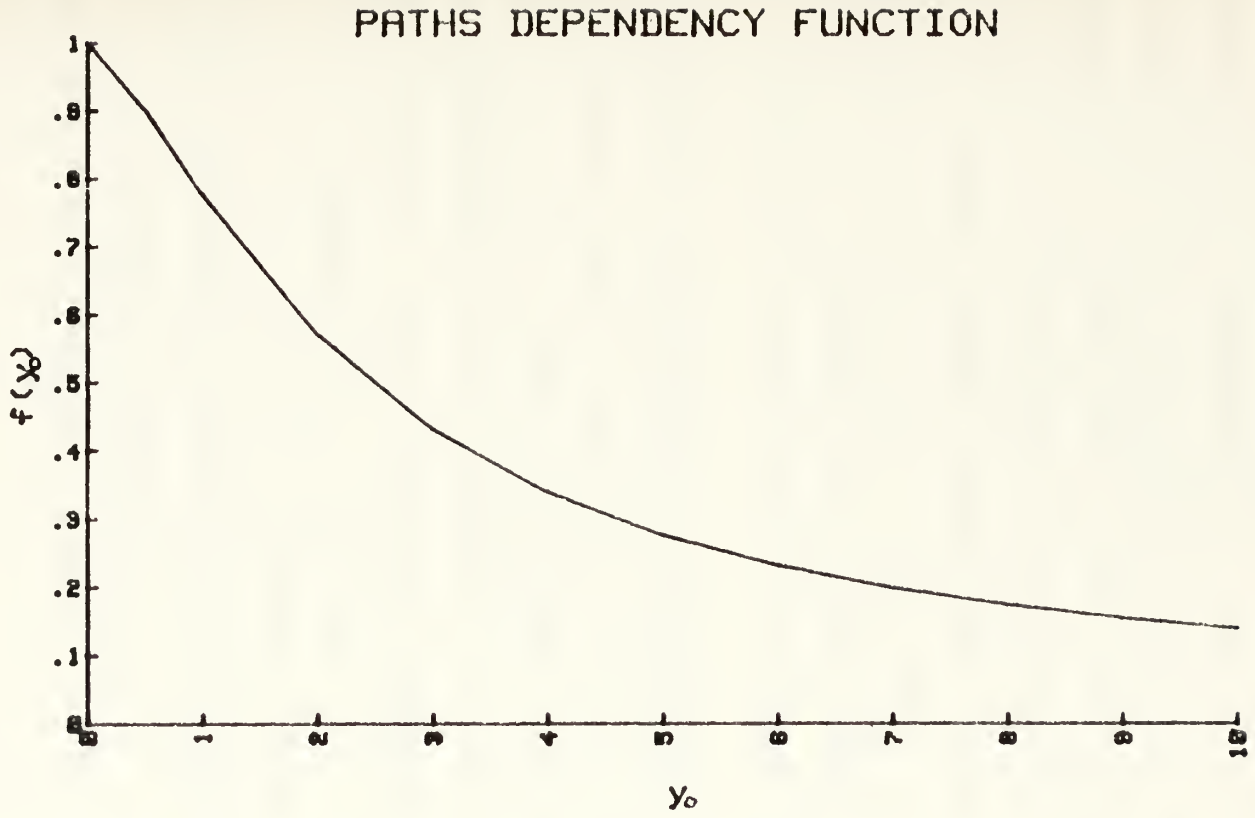


Figure 3. The behaviour of $f(y_0,\theta)$ (Eq. III-19) as a function of $y_0$ (for small $\theta$).

$$S_F^2(L,\theta) = \begin{cases} 2S_{2L}^2 & \theta = 0 \\ \\ S_{2L}^2 & \theta = \pi/4 \end{cases} \qquad \text{(III-20)}$$

These are the values of $S_F^2$ for the two extreme points of the transition region (from exact folding to statistical independence of the two parts of the folded path). In previous works on the subject of scintillation on folded paths, the authors assumed either exact folding or statistical independence of the two parts of the folded paths. Thus, as we pointed out in Section III-E, we can compare our results to those calculated by others, only at these two points.

## F. A CRITERION FOR STATISTICAL INDEPENDENCE

We have now enough information about the behaviour of $S_F^2(L,\theta)$, in order to define a practical criterion for statistical independence of the two parts of the folded path. Strictly speaking, the two parts are independent only for $\theta = \pi/4$. Yet because $f(y_0,\theta)$ decreases very fast at small $y_0$ and has a very long tail (approaches slowly to zero), we can define the region at which we have statistical independence, as the region in which $f(y_0,\theta) \leq e^{-1}$. From Figure 3 we see that this criterion is met (for small $\theta$).

$$y_0 \geq 4$$

Since

$$y_0 = \frac{L \sin(2\theta)}{L_0}$$

for small angles $\theta$, $y_0$ can be written as

$$y_0 \cong D/L_0$$

where D is the distance source-detector. Thus we see that the statistical independence between the two parts of the folded path depends on the distance source-detector, expressed in units of the outer scale.

As we said at the beginning of this section, one of the justifications for employing the path integral technique in our case, even though the main constraint on its utilization is violated at the point M, is the observation that the results in the extreme cases ($\theta = 0$; $\theta = \pi/4$) match the results which are obtained by other techniques.

For the case of $\theta = \pi/4$ we got

$$S_F^2(\theta = \pi/4) = S_{2L}^2$$

which is the expected result based on physical arguments and the results of Section III.D.

For the case of $\theta = 0$ we got

$$S_F^2(\theta = 0) = 2S_{2L}^2 = 4S_L^2 = (2S_L)^2$$

When a beam propagates back and forth along the same turbulent medium, the phase fluctuation due to each path element $\Delta x$ is doubled. Thus comparing the random variable S in the case of a path of length L ($S_L$) to the case of a folded path with $\theta = 0$ ($S_F$), we get

$$S_F = 2S_L$$

From probability theory, this gives for the variances

$$S_F^2 = 4S_L^2$$

which fits our results.

## IV. SCINTILLATION STRENGTH FOR THE FOLDED PATH

### A. THE RATIO BETWEEN THE SCINTILLATION STRENGTHS FOR THE FOLDED PATH AND THE ONE WAY PATH

The log intensity variance for the Rytov region for spherical waves is given by [1]

$$\sigma_\ell^2(L) = .5\, k^{7/6}\, C_n^2\, L^{11/6} \qquad \text{(IV-1)}$$

In the strong turbulence region (exponential distribution of I), the scintillation strength is given by the variance of the normalized intensity [8]

$$\sigma_I^2 = 1 + \frac{.69}{(\sigma_\ell^2)^{2/5}} \qquad \text{(IV-2)}$$

Comparing Eqs. (III-12) and (IV-1) we get for the Rytov region

$$\sigma_\ell^2(L) = \frac{6.31}{\pi^{3/2} k^{5/6} L_0^{5/3}}\, L^{5/6} S_L^2 \equiv A(k,L_0) L^{5/6} S_L^2 \qquad \text{(IV-3)}$$

or for a path of length 2L

$$\sigma_\ell^2(2L) = A\, 2^{5/6}\, L^{5/6}\, S_{2L}^2 \qquad \text{(IV-4)}$$

From Eq. (III-18) we get for the folded path

$$\sigma_\ell^2(F) = A\, 2^{11/6}\, L^{5/6}\, S_L^2 [1 + f(y_0, \theta)]$$

We can express the ratio between the folded path scintillation strength ($\sigma_\ell^2(F)$) and the one way scintillation strength ($\sigma_\ell^2(L)$), in the weak turbulence region, by

$$R = \frac{\sigma_\ell^2(F)}{\sigma_\ell^2(L)} = 2^{11/6}[1 + f(y_0,\theta)] \qquad \text{(IV-5)}$$

This ratio is the parameter which we are going to measure in the experimental part, in order to verify our model. The dependence of R on $y_0$ (for small $\theta$) is described in Figure 4.

B. DISCUSSION AND OBSERVATIONS

1. The Range of R and the Saturation of Scintillation Strength

As we can see from Eq. (IV-5) and the corresponding figure, the range of R is

$$2^{11/6} \leq R \leq 2^{17/6}$$

Therefore when we work with a system for which $\theta$ is close to zero or zero, we should expect the scintillation strength to be about seven times greater than the scintillation strength of the one-way path.

One should be aware of this large ratio especially while designing a system or an experiment which is based on the log-normal distribution. Since the region of the log-normal distribution, as we mentioned in Chapter II, is given by

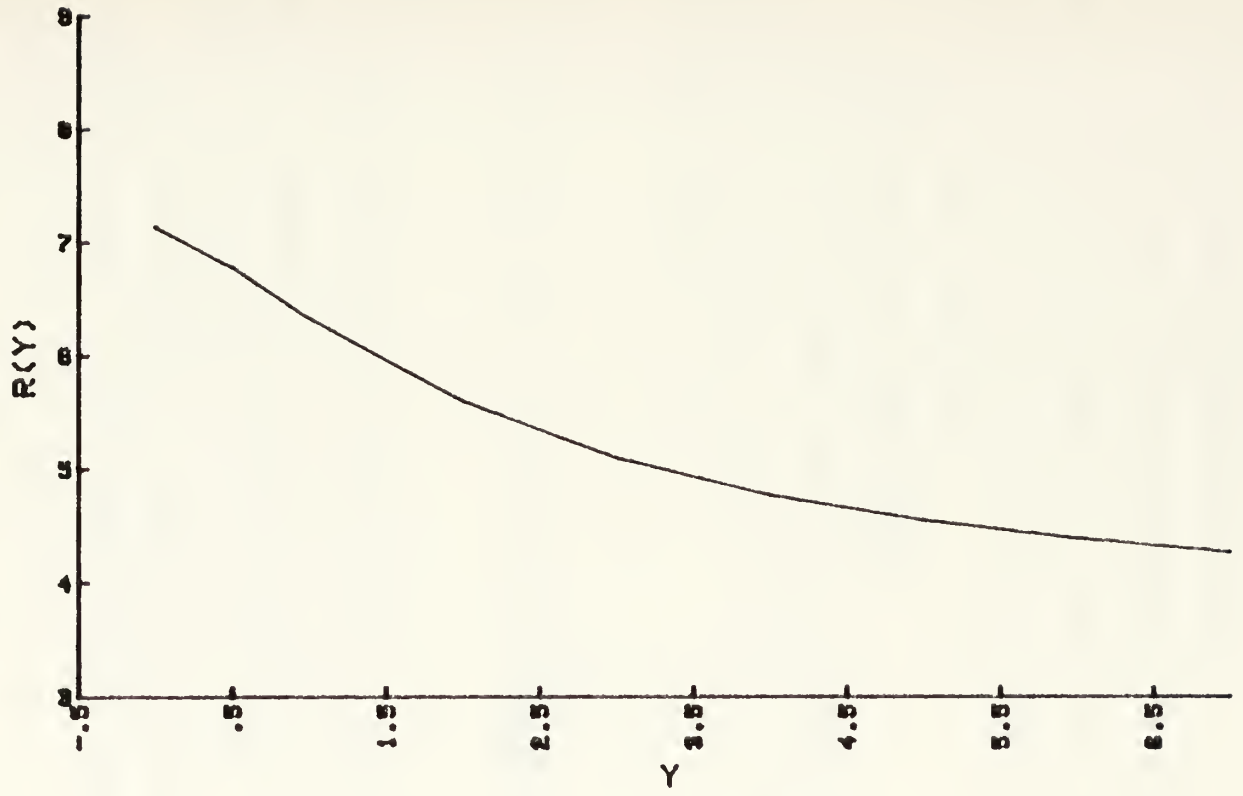


Figure 4. The ratio (R) between the scintillation strength for the folded path ($\sigma_\ell^2(F)$) and for the one way path $\sigma_\ell^2(L)$), as a function of $y_0$. (We assume small angles.)

$$\sigma_\ell^2 \lesssim 1$$

in the case of exact folding ($\theta = 0$), the upper limit of this region can be reached along relatively short distances and/or relatively weak turbulence levels.

On the other hand, since saturation can be achieved easily (relative to the one way case), it provides a way of carrying out experiments in the saturated region without the difficulties of using very long paths.

2. Comparison with Other Works

Smith [36,37] found that the scintillation strength of a spherical wave which propagates along a folded path (plane mirror) with $\theta = 0$ is

$$\sigma_\ell^2(F) = 64\pi^2 k^2 \int_0^L dx \int_0^\infty K\phi_n(K)\, \mathrm{Sin}^2\left[\frac{K^2 x(2L-x)}{4kL}\right] dK \qquad \text{(IV-6)}$$

Since he used the phase screen approach [6] and the Kolmogorov spectrum, his results are applicable only in the Rytov region and there is no dependence on the outer scale.

Using the Kolmogorov spectrum and the Mellin transform (formula 6.5(15) of Ref. [35], we get from Eq. (IV-6)

$$\sigma_\ell^2(F, \theta = 0) = A_3 \int_0^L dx \left[\frac{x(2L-x)}{L}\right]^{5/6}$$

where

$$A_3 = .033(4)2^{7/6}\,\Gamma(-5/6)(-1)\,\mathrm{Cos}(5\pi/12)\pi^2\,k^{7/6}\,C_n^2$$

Making the transformation

$$y = x/L$$

we get

$$\sigma_\ell^2(F,\ \theta = 0) = A_3\,L^{11/6}\int_0^1 dy[y(2-y)]^{5/6} \qquad \text{(IV-7)}$$

It is well known that for the one way path of length L [2]

$$\sigma_\ell^2(L) = 16\,\pi^2 k^2 \int_0^L dx \int_0^\infty K\phi_n(K)\,\mathrm{Sin}^2\left[\frac{K^2(L-x)}{2kL}\right]dK$$

Following the same steps as in the previous case, we get

$$\sigma_\ell^2(L) = A_4\int_0^L dx\left[\frac{x(L-x)}{L}\right]^{5/6}$$

where

$$A_4 = .033\ 4(-1)\,\Gamma(-5/6)\,\mathrm{Cos}(5\pi/12)\,\pi^2\,k^{7/6}\,C_n^2$$

and we can see that

$$A_3 = 2^{7/6} A_4$$

Taking $y = x/L$ we get

$$\sigma_\ell^2(L) = A_4 L^{11/6} \int_0^1 dy[y(1-y)]^{5/6} \qquad \text{(IV-8)}$$

From (IV-7) and (IV-8) we get

$$R = \frac{\sigma_\ell^2(F,\theta = 0)}{\sigma_\ell^2(L)} = \frac{A_3 \int_0^1 [y(2-y)]^{5/6} dy}{A_4 \int_0^1 [y(1-y)]^{5/6} dy}$$

Taking $y = 2x$ in the upper integral and observing that the integrand in the lower integral is a symmetric function about $y = 1/2$ we get

$$R = \frac{2^{7/6} A_4 \, 2 \, 4^{5/6} \int_0^{1/2} [x(1-x)]^{5/6} dx}{A_4 \, 2 \int_0^{1/2} [x(1-x)]^{5/6} dx} = 2^{17/6}$$

which is exactly the same results as we got by using the path integral technique.

It is easily seen that even though the results for $\theta = 0$ are the same (using the two techniques), Smith's paper cannot give the values of R for $\theta \neq 0$.

Gamo et al., [38] measured the value of R (for $\theta = 0$) along a path of 274m at night (using a collimated beam HeNe laser), to be 6.668. From their paper, it is not clear whether the measurements of $\sigma_\ell^2(L)$ and $\sigma_\ell^2(F)$ were done simultaneously.

3. The Weight Function in the Case of Exact Folding ($\theta = 0$)

The relative contribution to the scintillation of different points along the path is described by the weight function.

From Eqs. (IV-7) and (IV-8) we can see that the weight functions $W_i(x)$ for spherical waves are:

For one way $\quad W_L(x) = [x(1-x)]^{5/6}$

For the folded path $\quad W_F(x) = [x(2-x)]^{5/6}$

The two functions are shown in Figure 5.

From Figure 5 we can see that in the case of the folded path ($\theta = 0$), the main contribution to the scintillation comes from the vicinity of the mirror. In the case of the single path, the main contribution is from the center of the path. Since it is very unlikely that we can find the proper conditions under which $C_n^2(x)$ along an atmospheric path is constant, we should be careful when we compare results from the two types of path.

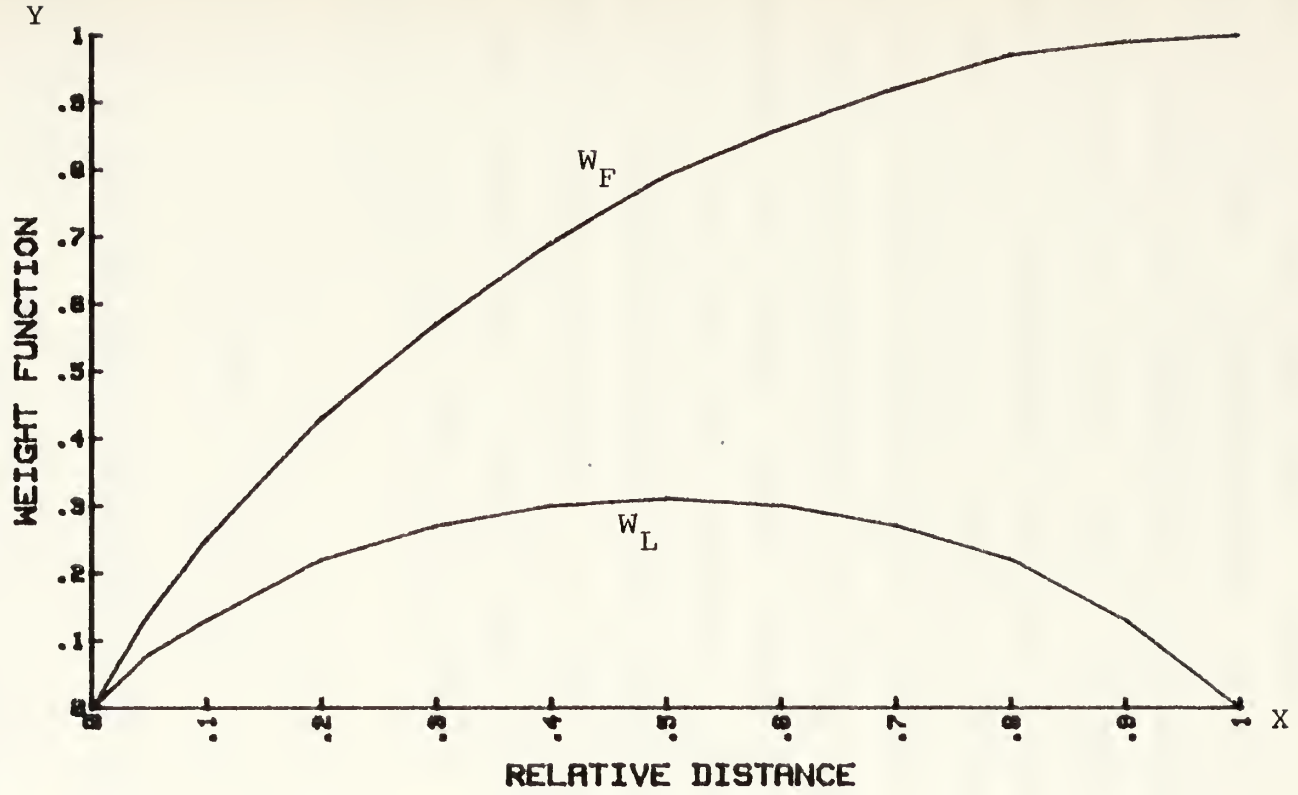


Figure 5. The weight functions of spherical waves in the cases of a single path ($W_L$) and a folded path with $\theta = 0$ ($W_F$). x represents the relative location along the path. For single path; the source at x = 0 and the detector at x = 1. For folded path; the source and the detector are at x = 0, the mirror is at x = 1.

## 4. The Effect of Path Folding on Aperture Averaging

The discussion and the evaluation of the scintillation strength in previous sections assumed that we have a point detector. The term point detector refers to a detector with aperture diameter ($D_d$) smaller than a critical length ($D_0$).

The aperture averaging can be explained qualitatively in the following way [7,40]. Due to atmospheric turbulence, the EM field at the detector plane has a certain spatial structure. This implies that the intensity (the modulus of the EM field) has a spatial structure too. In order to measure the full effect of the scintillation utilizing direct detection of intensity, the detector aperture should be smaller than the distance along which the intensity variations are negligible ($D_0$), otherwise the detector will average different intensities across its aperture. (In the language of Young [40], the detector will filter out the high spatial frequencies of the intensity's spatial variations.) The critical length is given by

$$B_I(D_0) = B_I(0)\, e^{-1}$$

where $B_I$ is the covariance function of the intensity at the detector plane.

It is well known [1,2] that in very weak turbulence

$$D_0 \sim \ell_F \equiv (\lambda L)^{1/2}$$

where $\lambda$ is wavelength and L is distance of propagation.

In the case of strong turbulence, it is not clear what is the exact value of $D_0$ [8]. The difficulty in obtaining the $D_0$ value arises from the difficulties in calculating the fourth moment of the EM field. Since the transverse correlation length of the EM field ($r_0$) [23] is a decreasing function of the distance whilst $\ell_F$ is an increasing one, at a certain distance the field and the intensity spatial covariance functions are dominated by $r_0$. Thus, beyond certain turbulence strength, $D_0$ should be a function of $r_0$.

As Yura [28] pointed out, the MCF of the EM field is proportional to the phase variance.

It follows from the above mentioned arguments that, as the phase variance increases the critical length $D_0$ decreases. Since we found that in the case of the folded path

$$S_F^2 = 2^{11/6}[1 + f(y_0,\theta)]\, S_L^2$$

it is obvious that while working with the folded path, we should utilize detector apertures which are much smaller than those which are used in the one way case.

# V. EXPERIMENTAL WORK

The main object of the experimental part is to measure the values of the function $R(y_0)$ and to compare them with the analytical function which is given in Eq. (IV-5).

In order to obtain the values of $R(y_0)$, we have to measure simultaneously the values of the one-way scintillation strength ($\sigma_L^2$) and the scintillation strength for the folded path ($\sigma_F^2$). These measurements should be done at several source-detector distances (assuming that $L_0$ is the same for all measurements).

## A. THE EXPERIMENTAL SYSTEM

The experimental system consists of two major parts:

1) The optical system;
2) Data reduction system.

### 1. The Optical System

The optical system is described in Figures 6 and 7.

The main problems which we dealt with during the planning and construction phases of our work were:

a) Selecting proper sources.
b) Making sure that the beams which propagate along the one-way path and the folded path see the same turbulence.
c) Obtaining high quality optical elements with relatively large apertures (within our budget and time span constraints).

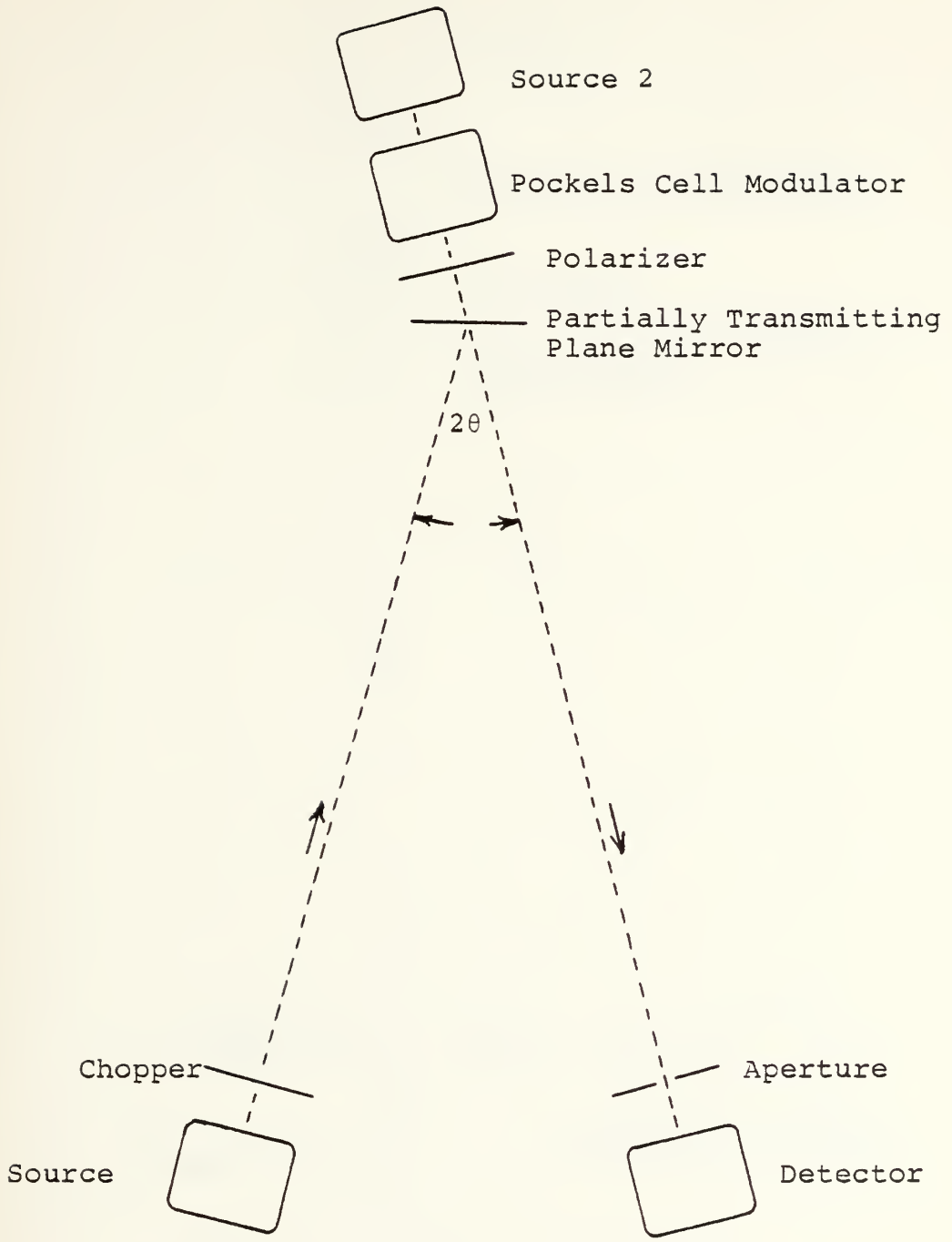


Figure 6. The optical system for measurements with $\theta \neq 0$.

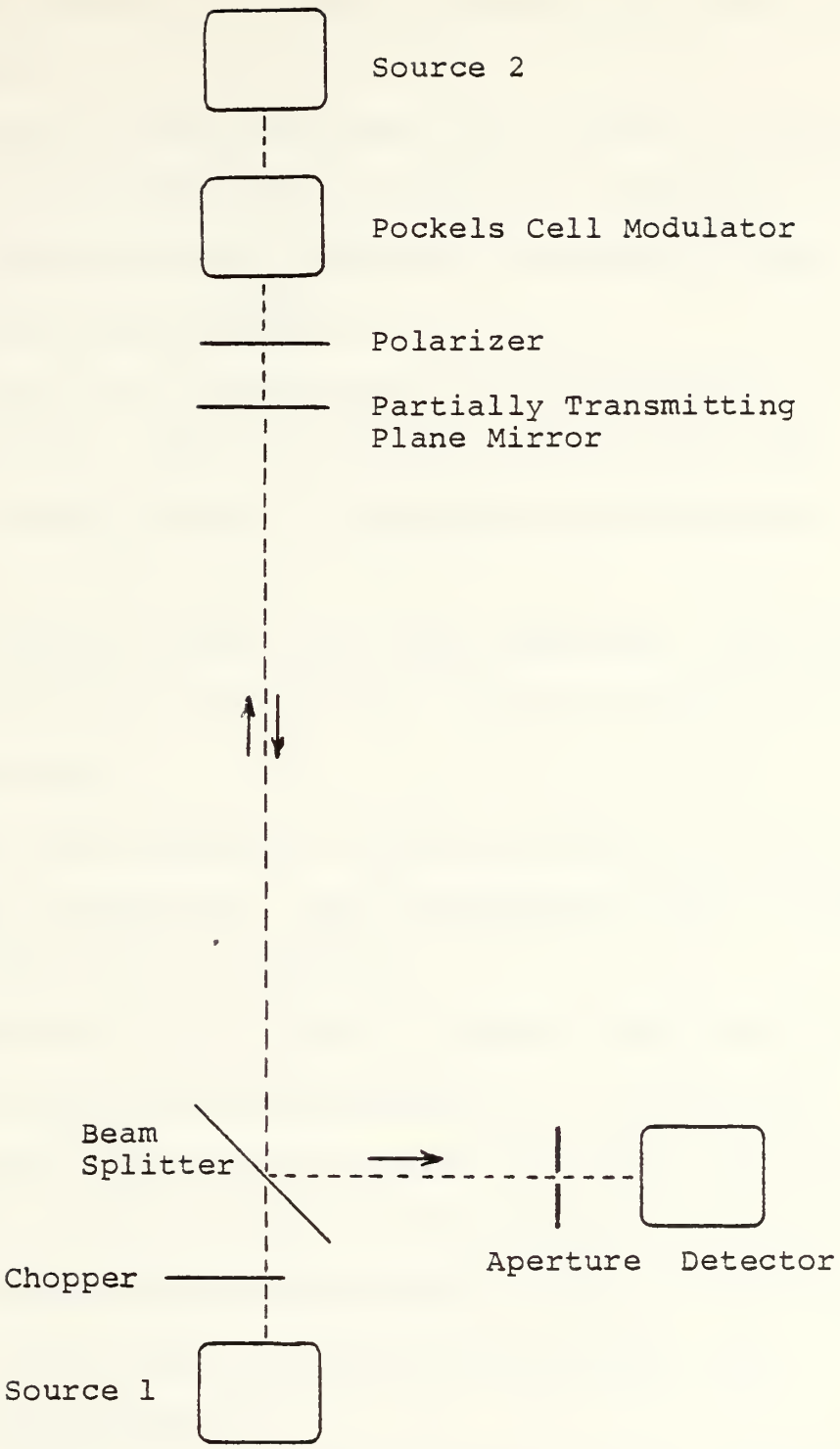


Figure 7. The optical system for $\theta = 0$.

The sources of our optical system should meet certain requirements:

a) Low noise. They should have low values of intensity variance in order not to obscure the intensity fluctuations due to the atmospheric turbulence along relatively short paths.

b) Operation in a pulsed mode or a simple way of modulation. (This requirement evolves from the way we were planning to subtract the background noise.)

c) When passing through the same turbulence, the respective measured scintillation strengths should be highly correlated.

d) Synchronized operation either in pulsed or modulated modes of operation. This requirement makes it possible to compare pairs of pulses.

Technically it is easy to employ a GaAs laser at the plane mirror end (the one-way source) in a pulsed mode, and a mechanically chopped HeNe laser at the other end (folded path source). These sources in these modes of operation, were used before by the Electro-Optics group of the Physics Department at the NPGS in previous experiments [41].

a. The Sources

It was found (assuming the sources' intensities are normally distributed) that the normal intensity variances of the sources were:

1) HeNe laser (Spectra Physics Model 155) mechanically chopped; $S_I^2 \leq 5 \times 10^{-4}$

2) 12 elements array of GaAs; $S_I^2 \leq 9 \times 10^{-4}$

3) 8x8 elements of GaAs; $S_I^2 \leq 5 \times 10^{-4}$. This laser matrix which is manufactured by Laser Diode Labs, was equipped with a Lucite parallelopiped rod mixing element, in order to enhance its output uniformity. This mixer was designed and built at the NPGS.

The conclusions from these measurements were:

1) In view of the expected levels of scintillation strength, all three lasers can be incorporated as sources in the optical system.

2) The 8x8 GaAs is a better (more stable) source than the 12 elements array GaAs. Therefore we decided to continue the experiments with the 8x8 GaAs laser only. In the following text, the term "GaAs laser" refers to this laser.

The correlation coefficient between the HeNe and the GaAs lasers were measured in a configuration which is described in Figure 8. The GaAs in a pulsed mode was triggered by the mechanical chopper via a pulse generator. In this way we were able to get interlaced series of pulses with a controlled time separation between them. For each laser we measured the log-intensity variance (in a way which will be described in Chapter V.B) and each pair of variances (one for each laser) was compared. For each run we calculated the

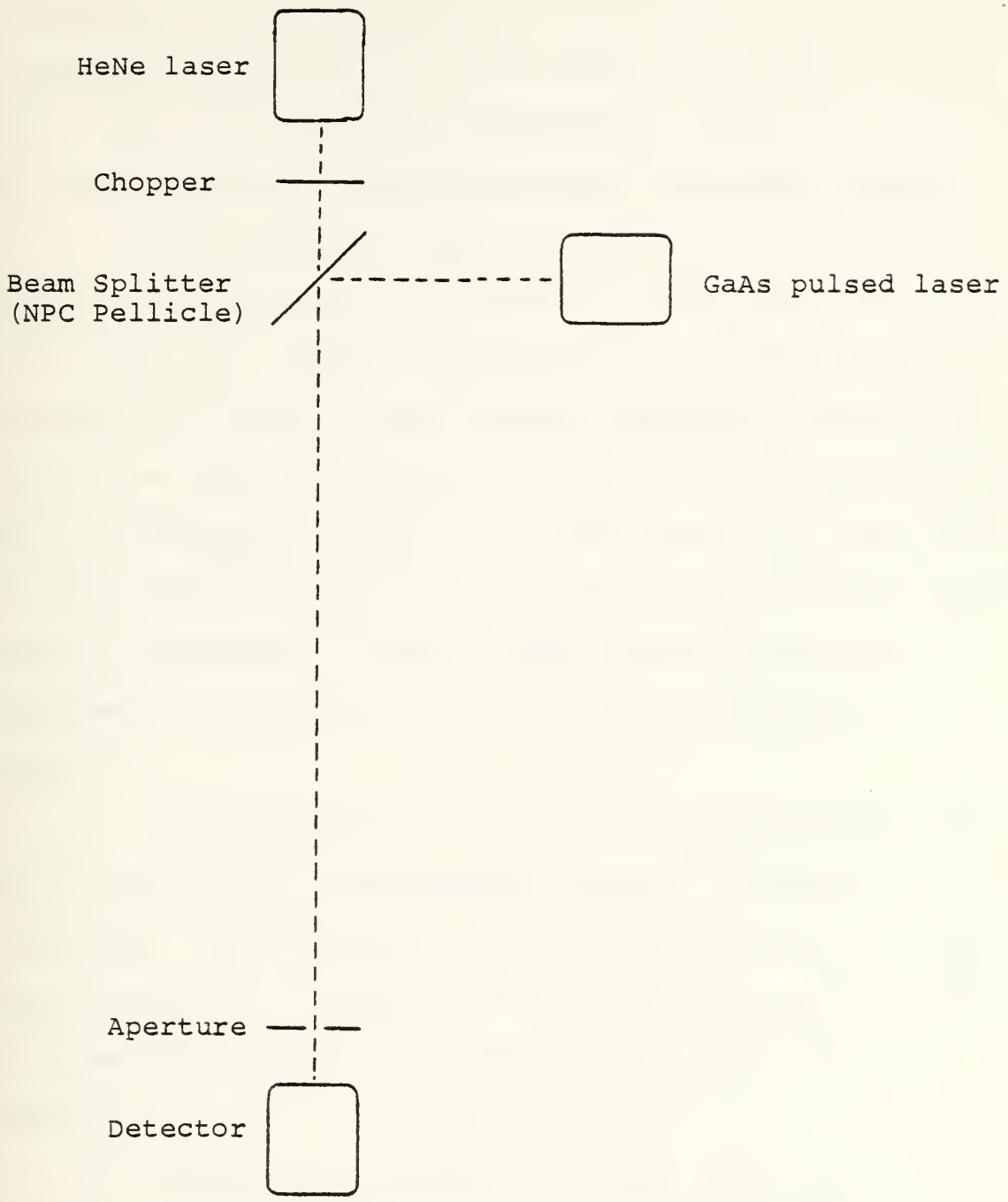


Figure 8. The configuration of the optical elements for the measurement of correlation coefficients

statistical correlation coefficient between the two series of variances' values. One run of this part of the experiment is described in Figure 9. In this particular run we got the highest value of correlation coefficient (.973). In the other runs the correlation coefficient values were much smaller.

As a result of this measurement, we decided to replace the GaAs laser with a second CW HeNe laser (similar to the first one), which is modulated by a Pockels cell modulator. (We tried to use a second mechanical chopper instead of the Pockel cell modulator but failed, because we were unable to synchronize it with the first one.) We found that the values of the two series of scintillation strengths (log-intensity variances) of the two HeNe lasers were highly correlated. A typical run with $\rho = .996$ is described in Figure 10.

The measurements of the correlation coefficients were carried out in the basement corridor of Spanagel Hall at the NPGS. (Its structure and turbulent features are described in Ref. 41.) The path length was 145 meters and the time separation between the pulses of the two lasers was 250-350 μs.

Based on the results of these experiments, we decided to continue our experiments with the two modulated CW HeNe lasers.

b. Frozen Atmosphere

As we mentioned in Chapter II of this paper, the atmosphere can be considered frozen for time intervals of

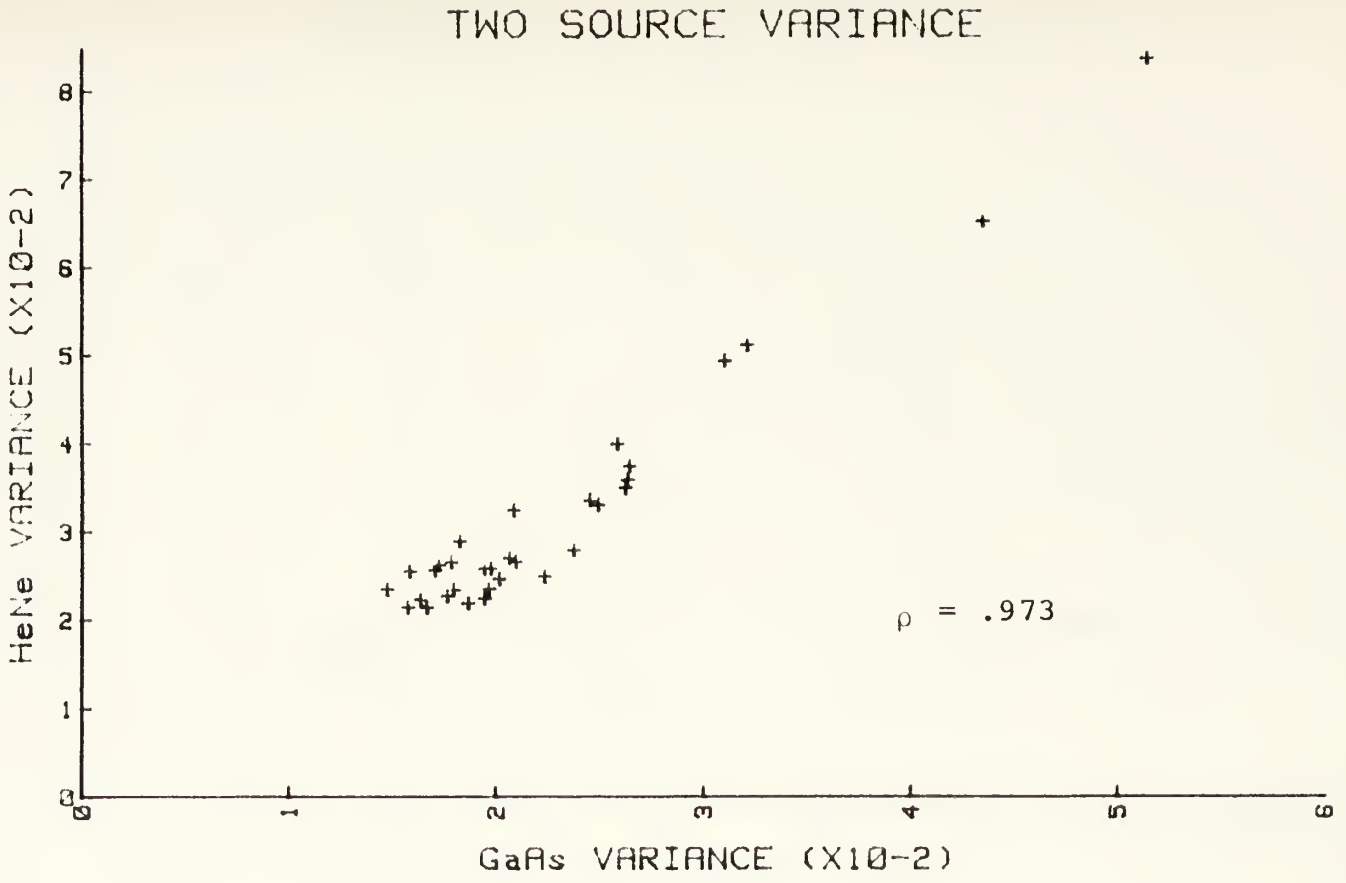


Figure 9. Correlation between the log normal intensity variances of the HeNe and the GaAs lasers which propagate along the same path. The value of the correlation coefficient $\rho$ is .973.

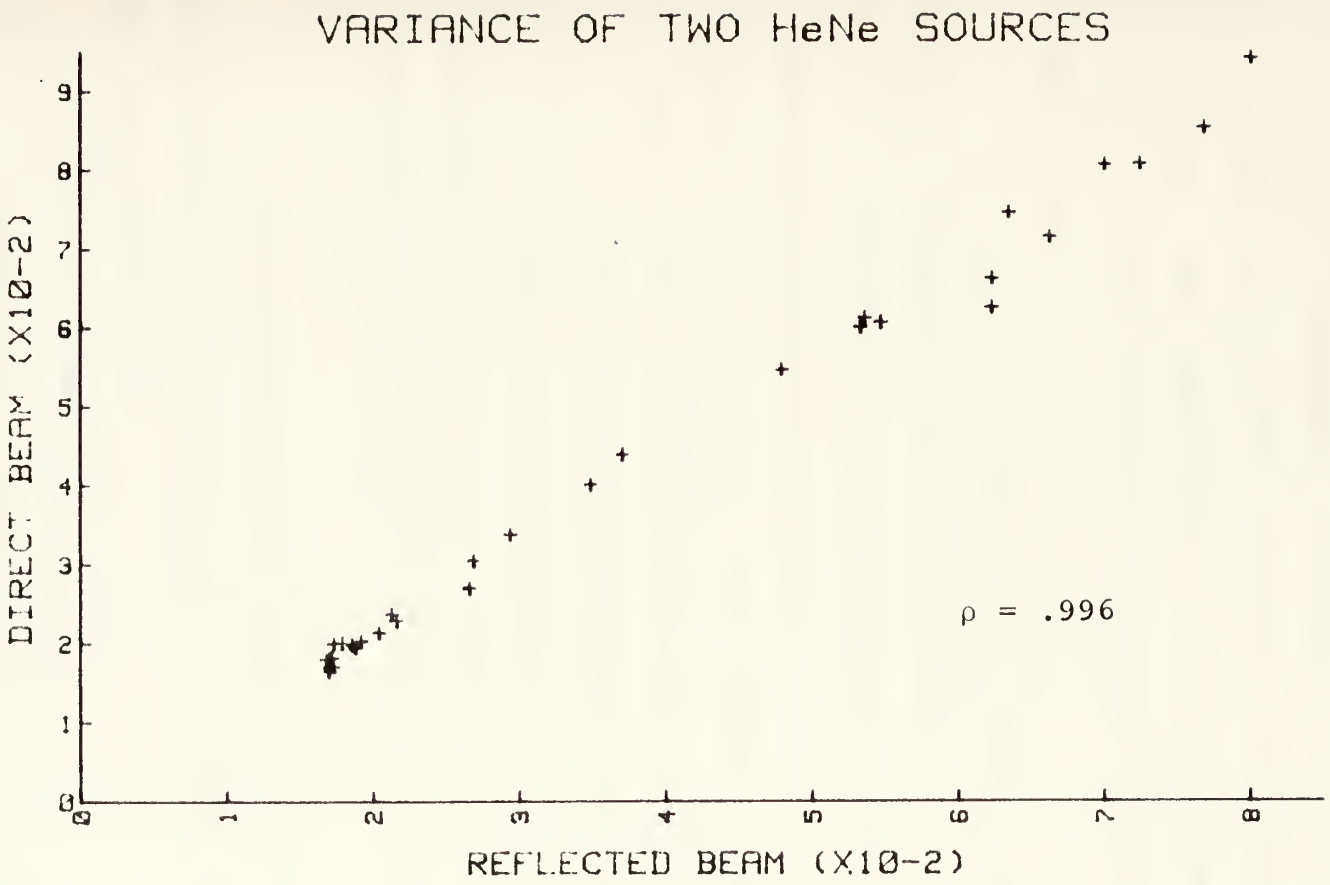


Figure 10. Correlation between the log normal intensity variances of two modulated CW HeNe lasers which propagate along the same path ($\rho$ = .996)

up to 1 ms. Since the round trip time of flight along the folded path (when the target is up to 10 km from the source) is less than 70 μs, the atmosphere can be taken to be frozen.

In our experiments we employ two interlaced series of pulses with a time separation ($\Delta t$) within each pair of pulses. The time separation in our system is dictated by the equipment which was available to us, and is not less than 250 μs.

We tested the assumption of frozen atmosphere by measuring the correlation coefficients of two series of log-intensity variances. The two series of pulses originated from one source by using two series of slits on the mechanical chopper for the HeNe laser, or by the use of the double output signal of the pulse generator, for the GaAs laser.

For the "double pulse" HeNe laser experiment with $t = 270$ μs, the correlation coefficient was $\rho = .998$. This experiment which was carried out in "the corridor" shows that for time separation of up to 270 μs, the atmosphere is frozen.

This experiment served also as final checkup for the equivalency of the two channels of the data reduction system (see Chapter V.B).

c. Optical Elements

We originally planned on doing the experiments with two targets; a plane mirror and a corner cube. The original configuration of the optical system was dictated by four major requirements:

1. High quality elements. To maintain the phase relation between different parts of the beam.
2. Large aperture elements. To intercept a large part of the beam, in order to avoid the effect of different transmitted/reflected intensities on the scintillation strength.
3. The laser at the target end (the one-way transmitter) cannot be placed behind the target, because its beam cannot be transmitted through the corner cube.
4. The beam-splitters in use should not cause an interference pattern.

The original configuration of the optical system is described in Figure 11.

The beam-splitters and the plane mirror target are made out of large pieces of flat fused Quartz, which were coated with Al, to achieve the required reflectivities, at the NPGS facilities. They were checked for flatness by interferometric techniques. A full description of the testing and coating processes is given in Reference 42.

The interference patterns due to the double reflection from the two surfaces of the beam-splitters, can be eliminated by applying an anti-reflection coating to one of the surfaces. Since we were not able to use this technique for various reasons, we used a different approach.

The beam-splitter at the detector end is located very close to the detector (5-10 cm). Hence, by using thick plates (taking apart the two secondary sources) we can eliminate

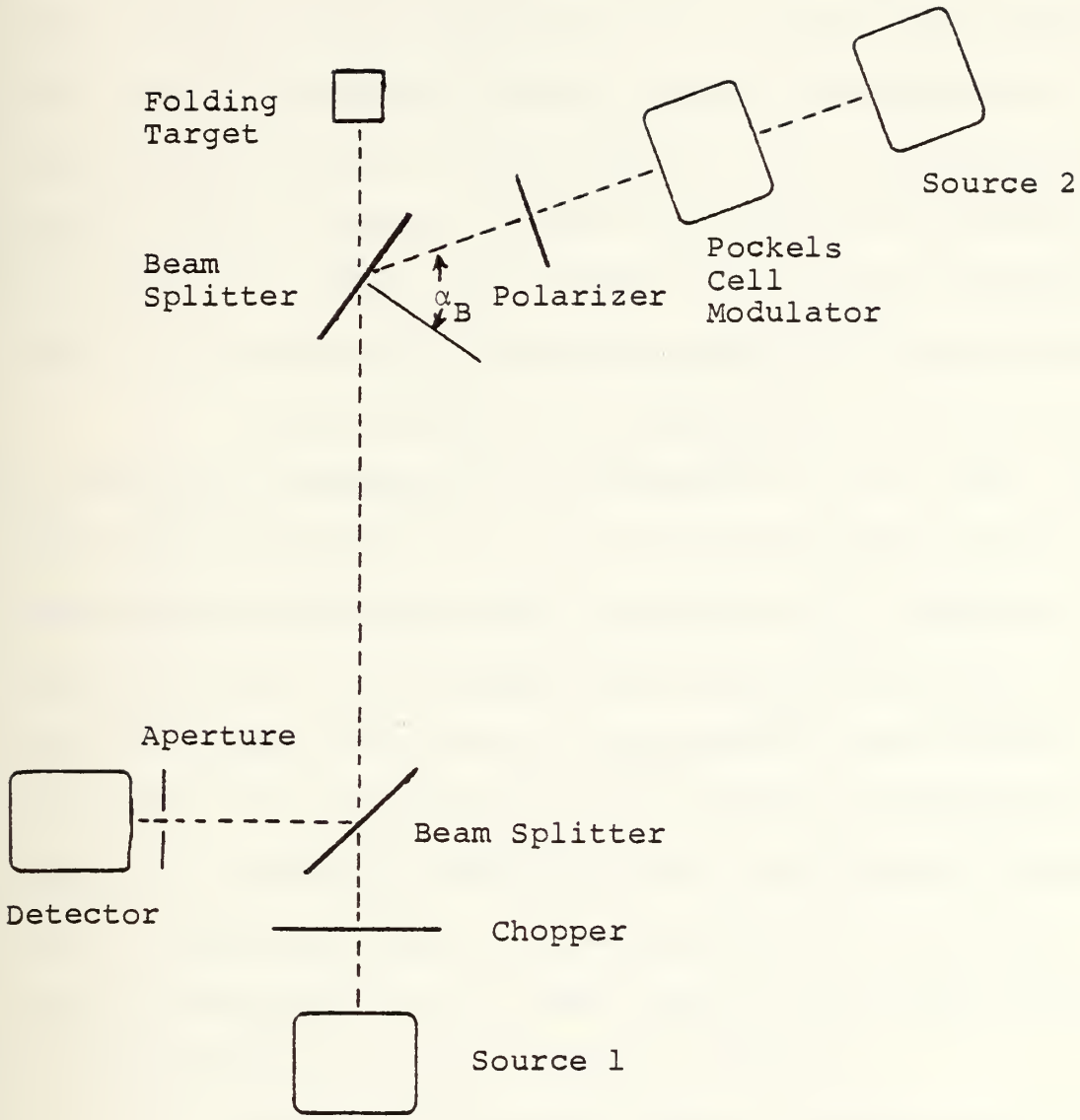


Figure 11. The original configuration of the optical system for measurements with $\theta = 0$. $\alpha_B$ is the Brewster angle.

this problem when the beam has a small angle of divergence. This beam-splitter thickness is 1/4", it has an elliptical shape (4 × 6"), and was coated to give a ratio of 1:2. The beam-splitter at the target end is a circular (6" diameter) plate of 1/2" thickness. As we can see from Figure 11, its interference pattern (at the detector) was eliminated by applying the Al coating to the back surface and working with a polarizer and angle of incidence equal to the Brewster angle, to eliminate the reflection from the front surface.

In the course of the experiments, it was found by observing the beams at the detector end, at night, that the beam which originates at $S_2$ is very homogeneous but the homogeneity of the beam that originates at $S_1$ suffers a great degradation due to its double pass through the Quartz beam-splitter at the target end. Since we use a back surface reflection for the first beam (it passes this beam-splitter twice too), the only explanation for the different effects on the two beams, is that the inhomogeneities in the beam-splitter material are of larger length scale than the diameter of the beam near the laser output aperture.

Because of the beam quality degradation, we changed the optical configuration from the one which is described in Figure 11, to the one which is described in Figure 6, utilizing the circular beam-splitter which has 70% reflectivity as the target mirror (with the coated surface facing the detector end).

As a result of the above mentioned change, we abandoned our original plan to measure the R values with a retroreflector as a target.

d. Other Elements

1) The mechanical chopper is constructed out of circular metal plate which is rotated at about 3000 rpm by an electrical motor. There are 20 slits on the circumference of the metal plate with a ratio of 1:4 between the slit's width and the opaque regions between them. The chopper modulates the CW HeNe laser beam at a frequency of about 1 kHz with "pulse" width (laser on) of about 200 μs. An LED (GaAs) and a detector which are placed on opposite sides of the chopper plate, provide a trigger signal at the same frequency as the laser modulation for the whole system. Due to this arrangement, we do not have to use a stabilized chopper.

2) The Pockels cell modulator is made by Coherent Associates (Model 3003).

3) The diameter of the aperture in front of the detector is 3 mm.

2. Data Reduction System

The data reduction system is described in Figure 12. It is a modification of a system which was used by the EO group for measuring the scintillation of one source. This system and its mode of operation are described in detail in Refs. [41, 42].

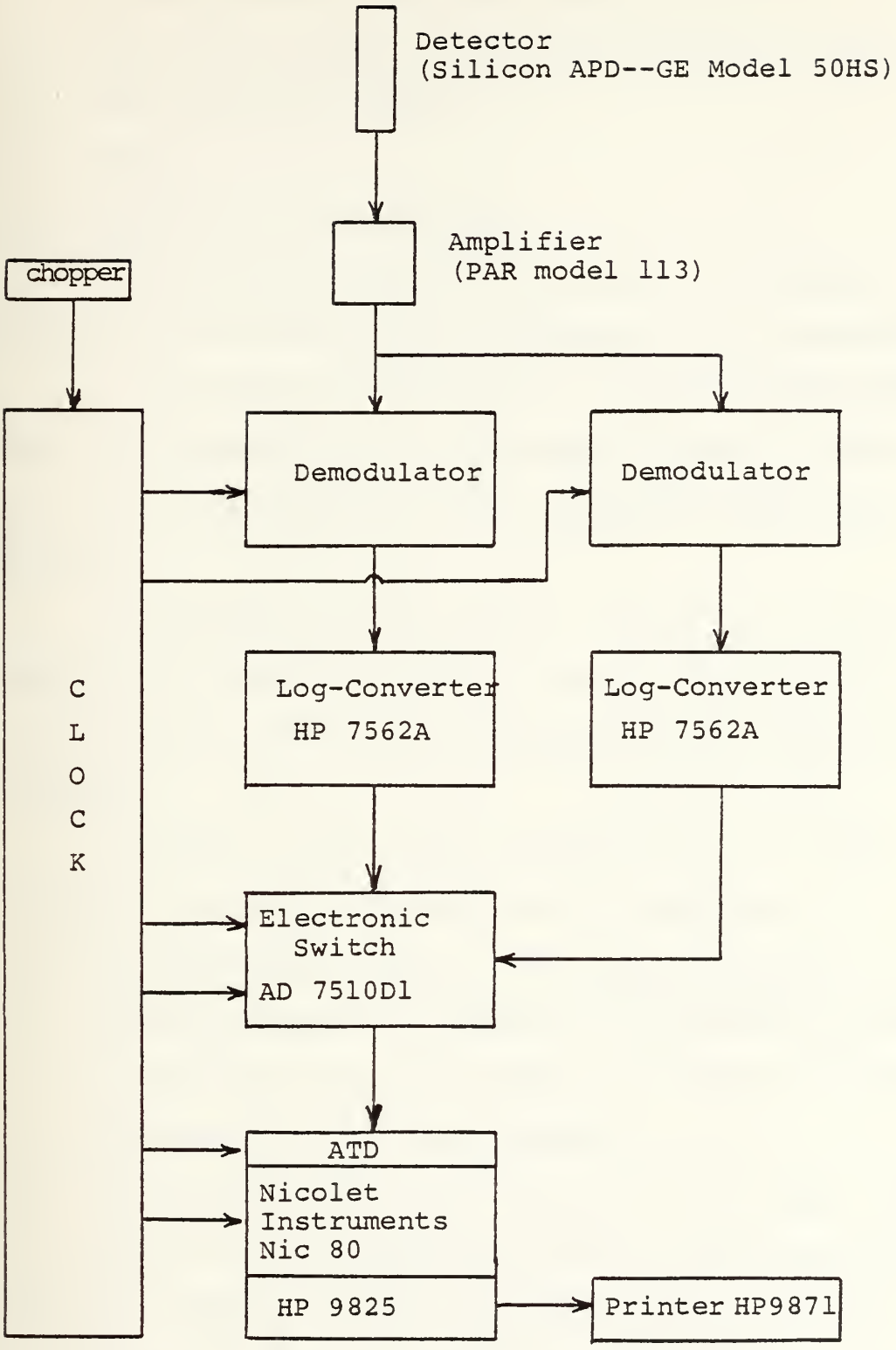


Figure 12. Data reduction system

The elements which were added by us are:

1. The second channel (demodulator and log converter).
2. The electronic switch.
3. Clock.
4. Software (for the Nic-80).

The electronic switch (AD 7510D1) alternately sends the signals from the parallel channels to the computer.

The clock is constructed of a set of pulse generators which are triggered by the mechanical chopper's LED-detector pair. The time sequence of the signals is described in Figure 13.

The change in the software enables us to store the measured log-intensity values of the two series in different storing spaces, for later calculation of the log-intensity variances.

The main steps which are carried out in each channel of the data reduction system, are the following:

1. The Demodulator samples the signal intensity and later (between pulses) it samples the background intensity. It subtracts the second from the first and sends this difference to the log-converter.
2. The log-converter takes the log of the input signal and sends it to the computer input via the electronic switch.
3. The computer samples the input signal, converts it from analog to digital and adds one to the proper counter. After sampling 16,384 pulses, it calculates the variance

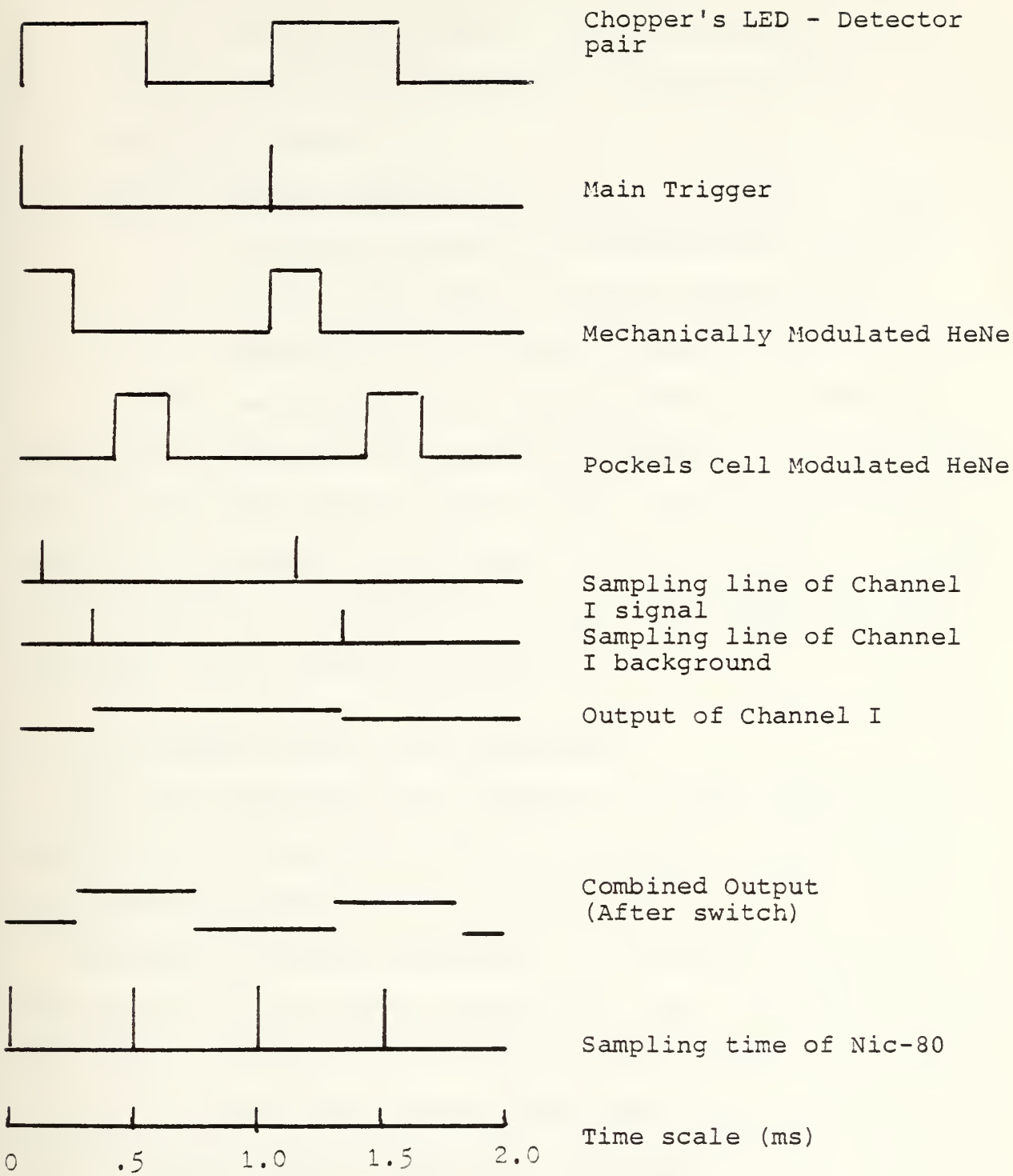


Figure 13. Time sequence of the system's signals

assuming that the distribution (after the conversion to log intensity was made by the log convertor) is normal. The calculated value is printed on the assigned printer.

Note: When we measured the sources' (lasers') normal intensity variances, we bypassed the log convertors, and used the average value of the intensity distribution to normalize it.

After we completed the modifications, we tested the two parallel channels for equality by comparing two series of pulses which came from the same laser. The high correlation coefficient between the variances of the two series ($\rho$ = .998) proves that the two channels are equal. The results of this experiment are described in Figure 14.

B. EXPERIMENTAL RESULTS AND DISCUSSION

The final experiment was carried out along a path of 62 meters on the lawns of the NPGS. The height of the optical path above the ground was 1.1 meters.

Because of weather conditions, we made measurements on February 27th and on March 3rd and 4th, 1982. Throughout the experiment, the weather was fair to clear. There were light winds (0-3 knots) from various directions, large portions of the path were shaded by high trees, and most of the time the grass was wet. The meteorological parameters which were taken from the NPGS meteorological station (measured at the NPGS) with other relevant parameters are summarized in Table I.

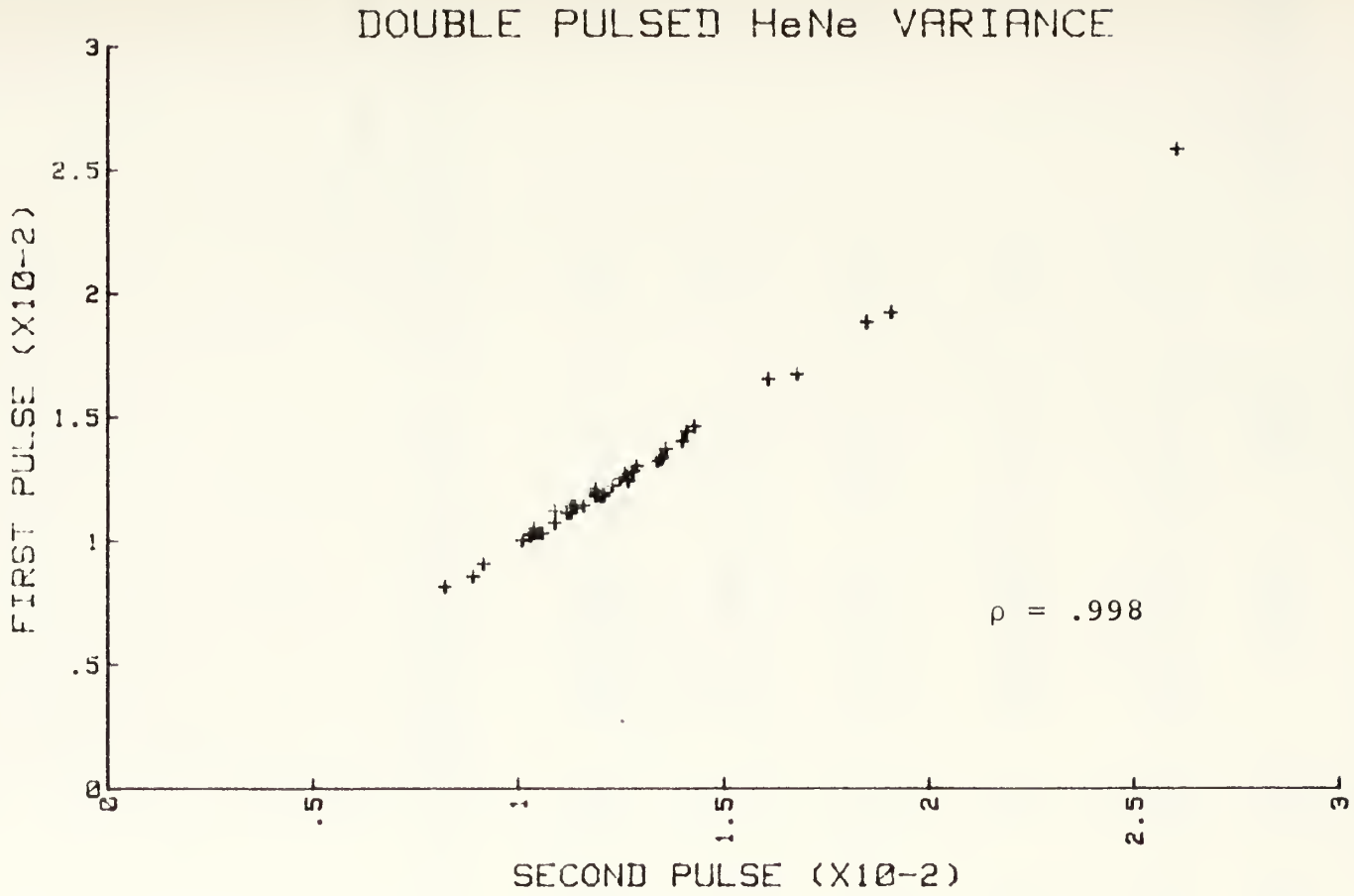


Figure 14. Correlation between the log intensity variances of the two series of pulses which originate from the same HeNe laser. The separation between the two series is 270 μs.

TABLE I

Information about the conditions under which the final experiment was done

| Distance Source Detector (cm) | R | Day | Time | T°F | RH% | Weather |
|---|---|---|---|---|---|---|
| 0 | 8.23 | 3-4-82 | 1237-1245 | 56 | 63 | Clear |
| 20 | 6.19 | 2-27-82 | 1626-1633 | 58 | 80 | Scattered clouds |
| 40 | 6.12 | 3-3-82 | 1447-1454 | 56 | 67 | Scattered clouds |
| 70 | 4.35 | 2-27-82 | 1239-1247 | 61 | 68 | Clear |
| 105 | 3.22 | 2-27-82 | 1053-1100 | 58 | 69 | Scattered clouds |

During all the runs, the wind was between 0-3 knots from various directions.

Figure 15 shows the experimental results, and the function $R(y_0,\theta)$ which is given in Eq. (IV-5).

The R value of each experimental point is an average of 16 measurements. Each measurement is the ratio of the log-intensity variances of the folded path (given distance source-detector) to the one way.

The $y_0$ values of the experimental points were calculated by

$$y_{0,i} = D_i/L_0$$

where $D_i$ is the distance source-detector (for the folded path), and $L_0$ was taken as 20 cm, to given an optimal fit with the analytical expression.

Even though we have only five experimental points, it seems that the experimental results match the analytical prediction quite well and confirm it.

The outer scale value ($L_0 \sim 20$ cm) which gives an optimal fit between the experimental results and the analytical prediction, seems to be relatively low, for a path which is 1.1 meters above the ground in an unstable surface layer. For a stable surface layer, this is a reasonable value [44].

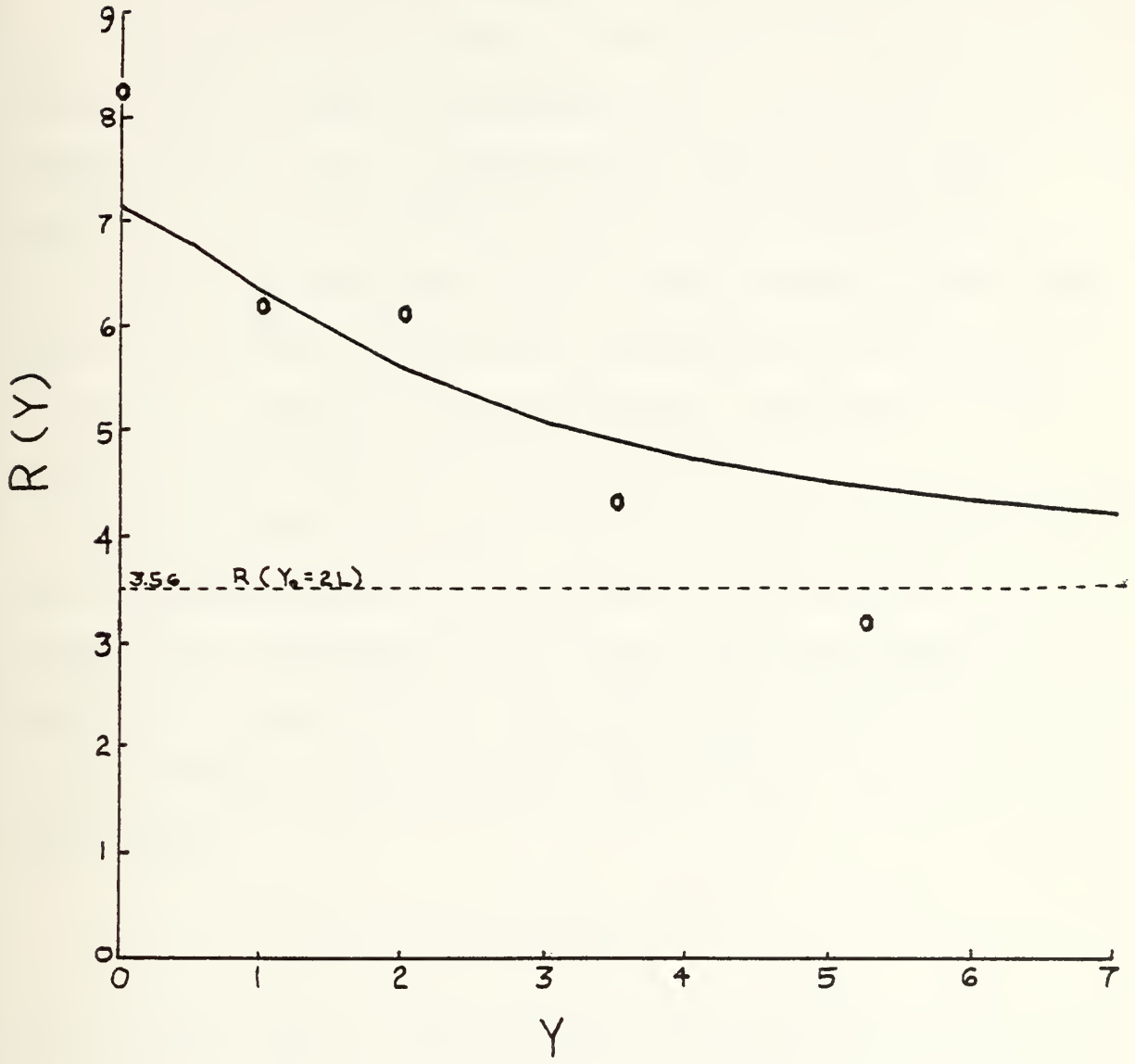


Figure 15. A comparison of the measured $R(y_0)$ values (o) with the analytical prediction (solid line)

## VI. SUMMARY

Optical scintillation along folded paths with different angles between the two parts of the path, is a part of the noise in many systems which measure the intensity of a reflected signal (e.g., a system which measures pollutant concentrations in the atmosphere via their absorption).

In previous works the scintillation strength along these types of paths was calculated by assuming either that the two parts of the path are statistically independent or by working with an "exact folding" ($\theta = 0$).

In this work we utilized the path integral technique and the Von Karman spectrum, to formulate a criterion for the statistical independence of the two parts (for spherical waves and a plane mirror). This criterion was given in terms of the distance source-detector expressed in the outer scale unit, namely

$$y_0 = D/L_0 \geq 4$$

For the same case, we developed an analytical expression for the ratio (R) of the log-intensity variances (folded path to one way path) as a function of $y_0$, in the Rytov region

$$R(y_0) = 2^{11/6}[1 + f(y_0)]$$

where

$$f(y_0) = \begin{cases} 0 & y_0 = 2L \text{ (L = the distance source-target)} \\ e^{-1} & y_0 \geq 4 \\ 1 & y_0 = 0 \text{ (exact folding)} \end{cases}$$

and showed that this prediction gives for the end points ($y_0 = 0, y_0 = 2L$) the same results which were predicted in other papers which dealt only with these points. Our approach gives an analytical prediction for intermediate values of $y_0$, which others do not.

In order to verify our predictions, we designed and put together an experimental system by modifying an existing data-reduction system, and constructing the optical system. This system enabled us to measure simultaneously the scintillation strength along a one-way and a folded path, which to the best of our knowledge, was never done before.

We measured $R(y_0)$ and found that

1) the maximum and the minimum values of $R(y_0)$ fit the analytical prediction well.
2) the slope of the experimental value fits well the predicted one, for an outer scale value $L_0 = 20$.

Based on these results, we think that our analytical expression predicts well the scintillation strength on folded paths.

## APPENDIX A

## THE SOLUTION OF EQUATION (III-11)

The right-hand side of Eq. (III-11)

$$S^2_{L_i} = A_1 \int_0^{L_i/L_0} dz\,(L_i/L_0 - z)\, z^{1/3}\, K_{1/2}(z)$$

is a difference of two integrals. The first one is

$$I_1 = A_1 L_i/L_0 \int_0^{L_i/L_0} dz\; z^{1/3} K_{1/3}(z)$$

and the second one is

$$I_2 = A_1 \int_0^{L_i/L_0} z^{4/3} K_{1/3}(z)$$

### The first integral

Using formula 7.14(6) of Ref. [43], we get

$$I_1 = A_1 (L_i/L_0)\, 2^{-2/3} \pi^{1/2} \Gamma(5/6)\, z\, [K_{1/3}(z) H_{-2/3}(z) + H_{1/3}(z) K_{-2/3}(z)] \Big|_0^{L_i/L_0} \qquad \text{(A-1)}$$

where $H_r(z)$ is the modified Struve function.

Equations 7.2(12), 7.2(13) and 7.5(57) of Ref. [43] give the following relationships.

$$I_r(z) = \sum_{m=0}^{\infty} (z/2)^{2m+r}/m!\Gamma(m+r+1) \qquad \text{(A-2)}$$

$$K_r(z) = \frac{\pi}{2\ \mathrm{Sin}(r\pi)}[I_{-r}(z) - I_r(z)] \qquad \text{(A-3)}$$

where $I_r(z)$ is the modified Bessel function of the first kind.

$$H_r(z) = \sum_{m=0}^{\infty} (z/2)^{2m+r+1}[\Gamma(m+3/2+r)\Gamma(m+3/2)]^{-1} \qquad \text{(A-4)}$$

For $z \to 0$, formulae (A-2) and (A-4) can be approximated by

$$I_r(z) = (z/2)^r/\Gamma(r+1) \qquad \text{(A-5)}$$

$$H_r(z) = (z/2)^{r+1}[\Gamma(3/2)\Gamma(3/2+r)]^{-1} \qquad \text{(A-6)}$$

Inserting (A-3), (A-5) and (A-6) in Eq. (A-1), and calculating the lower limit gives

$$\lim_{z\to 0} z[K_{1/3}(z)H_{-2/3}(z) + H_{1/3}(z)K_{2/3}(z)]$$

$$= \frac{\pi}{2} \lim_{z\to 0}\{\frac{1}{\sin(\pi/3)}[I_{-1/3}(z)-I_{1/3}(z)]H_{-2/3}(z)z$$

$$+ \frac{1}{\sin(2\pi/3)}[I_{-2/3}(z)-I_{2/3}(z)]H_{1/3}(z)z\}$$

$$= \pi/3^{1/2} \lim_{z\to 0}\{[(z/2)^{-1/3}/\Gamma(2/3)-(z/2)^{1/3}/\Gamma(4/3)]$$

$$\times (z/2)^{1/3}[\Gamma(3/2)\Gamma(5/6)]^{-1}$$

$$+ [(z/2)^{-2/3}/\Gamma(1/3)-(z/2)^{2/3}/\Gamma(5/3)]$$

$$\times [(z/2)^{4/3}[\Gamma(3/2)\Gamma(11/6)]^{-1}]\}z$$

$$= \pi/3^{1/2} \lim_{z\to 0}\{az-b\ z^{5/3} + cz^{5/3} - dz^{3}\}$$

where a, b, c and d are constants.

Thus for z = 0

$$z[K_{1/3}(z)H_{-2/3}(z) + H_{1/3}(z)K_{2/3}(z)] = 0 \qquad \text{(A-7)}$$

For large z, formulae 7.13(7), 7.5(52), 7.5(63) and 7.13(4) of Ref. [43] give, up to $0(z^{-2})$,

$$K_r(z) = (\pi/2z)^{1/2}e^{-z}[1 + \frac{\Gamma(3/2+r)}{\Gamma(r-\frac{1}{2})}(2z)^{-1} + 0(z^{-2})] \qquad \text{(A-8)}$$

$$H_r(z) = \frac{e^z z^{-1/2}}{\sqrt{2\pi}}\left[1 - \frac{\Gamma(3/2+r)}{\Gamma(\frac{1}{2}+r)}(2z)^{-1} + 0(z^{-2})\right] \qquad \text{(A-9)}$$

$$- \frac{1}{\pi}\left[\sum_{m=0}^{N-1} (-1)^m \frac{\Gamma(m+\frac{1}{2})}{\Gamma(r+\frac{1}{2}-m)}(z/2)^{r-2m-1} + 0(z^{r-2N-1})\right]$$

Using Eqs. (A-8) and (A-9) in the upper limit of Eq. (A-1), we get ($z = L_i/L_0 \gg 1$)

$$z[K_{1/3}(z)H_{-2/3}(z) + H_{1/3}(z)K_{2/3}(z)]$$

$$= (\pi z/2)^{1/2} e^{-z}\{[1 + \frac{\Gamma(11/6)}{\Gamma(-1/6)}(2z)^{-1} + 0(z^{-2})]$$

$$\times \left[\frac{e^z z^{-1/2}}{\sqrt{2\pi}}\left[1 - \frac{\Gamma(5/6)}{\Gamma(-1/6)}(2z)^{-1} + 0(z^{-2})\right]\right.$$

$$\left. - \frac{1}{\pi}\left[\frac{\Gamma(\frac{1}{2})}{\Gamma(-1/6)}(z/2)^{-5/3} + 0(z^{-11/3})\right]\right]$$

$$+ \left[1 + \frac{\Gamma(13/6)}{\Gamma(1/6)}(2z)^{-1} + 0(z^{-2})\right]$$

$$\times \left[\frac{e^z z^{-1/2}}{\sqrt{2\pi}}\left[1 - \frac{\Gamma(11/6)}{\Gamma(5/6)}(2z)^{-1} + 0(z^{-2})\right]\right.$$

$$\left. - \frac{1}{\pi}\left[\frac{\Gamma(\frac{1}{2})}{\Gamma(5/6)}(z/2)^{-2/3} + 0(z^{-8/3})\right]\right]$$

$$= \frac{1}{2}\{2 + \left[\frac{\Gamma(11/6)}{\Gamma(-1/6)} - \frac{\Gamma(5/6)}{\Gamma(-1/6)} + \frac{\Gamma(13/6)}{\Gamma(5/6)} - \frac{\Gamma(11/6)}{\Gamma(5/6)}\right](2z)^{-1}$$

$$+ 0(z^{-2})\} - e^{-z}[az^{1/2} + (\text{smaller powers of } z)]$$

where a is a constant.

Thus for $z \geq 10$, the last term is negligible and

$$z[K_{1/3}(z)H_{-2/3}(z) + H_{1/3}(z)K_{2/3}(z)] \qquad \text{(A-10)}$$

$$= 1 + \frac{1}{4}\left[\frac{\Gamma(13/6)}{\Gamma(5/6)} - \frac{17}{18}\right]z^{-1} + 0(z^{-2})$$

Inserting Eqs. (A-7) and (A-10) in Eq. (A-1), we get for $L_i/L_0 \geq 10$

$$I_1 = \frac{A_1(L_i/L_0)\pi^{1/2}\Gamma(5/6)}{2^{2/3}}\left\{1 + \frac{1}{4}\left[\frac{\Gamma(13/6)}{\Gamma(5/6)} - \frac{17}{18}\right](L_i/L_0)^{-1}\right.$$

$$\left. + 0((L_i/L_0)^{-2})\right\} \qquad \text{(A-11)}$$

The second integral

Using formula 7.14(3) of Ref. [43], we get

$$I_2 = A_1[-z^{4/3}K_{4/3}(z)]\Big|_0^{L_i/L_0}$$

For the upper limit we make use of Eq. (A-8) and we get, up to $z^{-2}(L_i/L_0 = z >> 1)$

$$z^{4/3}K_{4/3}(z) = \left(\frac{\pi}{2}\right)^{1/2}z^{5/6}e^{-z}\left[1 + \frac{\Gamma(17/6)}{\Gamma(5/6)}(2z)^{-1} + 0(z^{-2})\right]$$

which for $L_i/L_0 = z \geq 10$ is almost zero (less than $10^{-3}$). For the lower limit, by use of Eqs. (A-2) and (A-5)

$$\lim_{z\to 0} z^{4/3}K_{4/3}(z) = \frac{\pi}{2\,\mathrm{Sin}(4\pi/3)} \lim_{z\to 0}[2^{4/3}/\Gamma(-1/3) - az^{8/3}]$$

$$= \frac{\pi\, 2^{1/3}}{\mathrm{Sin}(4\pi/3)\Gamma(-1/3)}$$

Thus for $L_i/L_0 \geq 10$

$$I_2 = \frac{A_1\, \pi\, 2^{1/3}}{\mathrm{Sin}(4\pi/3)\Gamma(-1/3)} \qquad \text{(A-12)}$$

We can now write the solution of Eq. (III-11)

$$S^2_{L_i} = A_1\{\frac{(L_i/L_0)\pi^{1/2}\Gamma(5/6)}{2^{2/3}}[1 + \frac{1}{4}[\frac{\Gamma(13/6)}{\Gamma(5/6)} - \frac{17}{18}](L_i/L_0)^{-1}$$

$$+ 0(L_i/L_0)^{-2}) - \frac{\pi\, 2^{1/3}}{\mathrm{Sin}(4\pi/3)\Gamma(-1/3)}\}$$

$$S^2_{L_i} = \frac{A_1\, \pi^{1/2}\, \Gamma(5/6)}{2^{2/3}}(L_i/L_0)\{1 + [\frac{1}{4}[\frac{\Gamma(13/6)}{\Gamma(5/6)} - \frac{17}{18}] \qquad \text{(A-13)}$$

$$- \frac{2\,\pi^{1/2}}{\mathrm{Sin}(4\pi/3)\Gamma(-1/3)\Gamma(5/6)}(L_i/L_0)^{-1} + 0((L_i/L_0)^{-2})\}$$

## APPENDIX B

## NUMERICAL EVALUATION OF $f(y_0,\theta)$

The equation for $f(y_0,\theta)$ is

$$f(y_0,\theta) = \frac{A_2}{y_0} \int_0^{\pi/2-\theta} d\alpha \int_0^{y_1} y^{4/3} K_{1/3}(y)\, dy$$

As we showed in Appendix A,

$$\int_0^{y_1} y^{4/3} K_{1/3}(y)\, dy = -y^{4/3} K_{4/3}(y) \Big|_0^{y_1} \qquad (1)$$

$$\lim_{y\to 0} y^{4/3} K_{4/3}(y) = \frac{\pi\, 2^{1/3}}{\mathrm{Sin}(4\pi/3)\,\Gamma(-1/3)} \qquad (2)$$

Thus

$$f(y_0,\theta) = \frac{A_2}{y_0} \int_0^{\pi/2-\theta} d\alpha \left[B - y_1^{4/3} K_{4/3}(y_1)\right]$$

where

$$B = \frac{\pi\, 2^{1/3}}{\mathrm{Sin}(4\pi/3)\,\Gamma(-1/3)} \qquad (B\text{-}1)$$

or

$$f(y_0,\theta) = \frac{A_2}{y_0}\left[B(\pi/2-\theta) - I_5(y_0,\theta)\right] \qquad (B\text{-}2)$$

where

$$I_5(y_0,\theta) = \int_0^{\pi/2-\theta} d\alpha\ y_1^{4/3}K_{4/3}(y_1)$$

and

$$y_1 = y_0/\mathrm{Sin}(2\theta+\alpha)$$

Taking

$$\beta = 2\theta+\alpha$$

we get

$$I_5(y_0,\theta) = \int_{2\theta}^{\pi/2} d\beta y_1^{4/3}K_{4/3}(y_1) + \int_{\pi/2}^{\pi/2+\theta} d\beta y_1^{4/3}K_{4/3}(y_1)$$

From

$$y_1 = y_0/\mathrm{Sin}\ \beta$$

we get

$$dy_1 = -\frac{y_0\ \mathrm{Cos}\ \beta}{\mathrm{Sin}^2\beta}\, d\beta$$

Therefore, for the first integral in $I_5$

$$d\beta = - \left|\frac{\sin^2\beta}{\cos\beta}\right| \frac{dy_1}{y_0}$$

and for the second integral

$$d\beta = \left|\frac{\sin^2\beta}{\cos\beta}\right| \frac{dy_1}{y_0}$$

Since

$$\left|\frac{\sin^2\beta}{\cos\beta}\right| = \frac{\sin^2\beta}{(1-\sin^2\beta)^{1/2}} = \frac{y_0^2}{y_1(y_1^2 - y_0^2)^{1/2}},$$

$$I_5(y_0,\theta) = y_0 \int_{y_0}^{y_a} \frac{y^{1/3}K_{4/3}(y)}{(y^2 - y_0^2)^{1/2}}\, dy + y_0 \int_{y_0}^{y_b} \frac{y^{1/3}K_{4/3}(y)}{(y^2 - y_0^2)^{1/2}}\, dy$$

where

$$y_0 = L \sin(2\theta)/L_0 \qquad \text{(B-3-a)}$$

$$y_a = y_0/\sin(2\theta) = L/L_0 \qquad \text{(B-3-b)}$$

$$y_b = y_0/\sin(\pi/2-\theta) = y_0/\cos\theta = \frac{2L \sin\theta}{L_0} \qquad \text{(B-3-c)}$$

Integrating by parts (making use of formula 7.14(3) of Ref. [43] gives

$$\int_{Y_0}^{Y_i} \frac{y^{4/3}K_{4/3}(y)}{y(y^2 - y_0^2)^{1/2}}\,dy = \frac{1}{y_0}\left[\mathrm{Sec}^{-1}(y/y_0)\,y^{4/3}K_{4/3}(y)\Big|_{y_0}^{Y_i} + \int_{Y_0}^{Y_i} \mathrm{Sec}^{-1}(y/y_0)\,y^{4/3}K_{1/3}(y)\right]$$

Since

$$\mathrm{Sec}^{-1}(1) = 0,$$

$$\mathrm{Sec}^{-1}(y_a/y_0) = \pi/2-2\theta,$$

$$\mathrm{Sec}^{-1}(y_b/y_0) = \theta,$$

and

$$y^{4/3}K_{4/3}(y)$$

has a finite value,

$$I_5(y_0,\theta) = -\left[(\pi/2-2\theta)y_a^{4/3}K_{4/3}(y_a) + \theta y_b^{4/3}K_{4/3}(y_b) - \int_{Y_0}^{Y_a} g(y)\,dy - \int_{Y_0}^{Y_b} g(y)\,dy\right.$$

where

$$g(y) = \mathrm{Sec}^{-1}(y/y_0)\,y^{4/3}K_{1/3}(y). \qquad \text{(B-4)}$$

Hence

$$f(y_0,\theta) = \frac{A_2}{y_0}[B(\pi/2-\theta) + (\pi/2-\theta)y_a^{4/3}K_{4/3}(y_a) \qquad \text{(B-5)}$$

$$+ \theta y_b^{4/3}K_{4/3}(y_b) - \int_{y_0}^{y_a} g(y)\,dy - \int_{y_0}^{y_b} g(y)\,dy$$

This the exact form of $f(y_0,\theta)$.

From the definition of $y_a$ (Eq. (B-3-b)) we can see that in all practical situations, when the path of propagation is parallel to the ground but not too high, we can take $y_a >> 1$.

Using formula 7.13(7) of Ref. [43], we get for $y >> 1$

$$y^{4/3}K_{4/3}(y) = (\pi/2)^{1/2}y^{5/6}e^{-y}\left[\sum_{m=0}^{N-1}\frac{\Gamma(11/6+m)}{m!\Gamma(11/6-m)}(2y)^{-m} + 0(y^{-N})\right]$$

$$= (\pi/2)^{1/2}y^{5/6}e^{-1}[1 + (55/72)y^{-1} + 0(y^{-2})]$$

By taking only the first two terms in the brackets, the error in the value of $y^{4/3}K_{4/3}(y)$ is less than 1% for $y \geq 10$. Thus for $y \geq 10$ we can take

$$y^{4/3}K_{4/3}(y) \cong (\pi/2)^{1/2}y^{5/6}e^{-y}[1 + (55/72)y^{-1}]$$

$$\leq (2\pi)^{1/2}y^{5/6}e^{-y}$$

Comparing this expression with B, we find

$$B/1000 > y^{4/3}K_{4/3}(y) \qquad \text{for } y \geq 10$$

Since in Eq. (B-5), B and $y_a^{4/3}K_{4/3}(y_a)$ have the same coefficient $(\pi/2-\theta)$, we can approximate this equation by

$$f(y_0,\theta) \cong \frac{A_2}{y_0}[B(\pi/2-\theta) + \theta y_b^{4/3}K_{4/3}(y_b) \qquad \text{(B-6)}$$

$$- \int_{y_0}^{y_a} g(y)dy - \int_{y_0}^{y_b} g(y)dy]$$

Numerical Evaluation

The numerical evaluation of Eq. (B-6) was done in the Computer Center of the NPGS, on an IBM 3033. The program is written in FORTRAN IV and is given at the end of this appendix.

The important information about the program is listed below.

1) The function $f(y_0,\theta)$ is evaluated with $y_0$ as the independent variable. The step by which $y_0$ is changed, is determined by a constant (parameter) of the program.
2) The angle $\theta$ is calculated from the equation

$$\theta = \frac{1}{2}\,\mathrm{Sin}^{-1}(L_i/y_0)$$

3) The parameter $L_1$ which is given for each run, is the distance source-mirror in units of the outer scale.

$$L_i = L/L_0$$

4) The constants $A_2$, B are constants of the program. Their values, which were calculated from Eqs. (III-19) and (B-1), are

$$A_2 = .7934 \qquad B = 1.1250$$

5) The values of the modified Bessel function of the third kind $K_r(y)$, are calculated in different ways for the two regions:

(a) $0.1 \leq y \leq 4$

(b) $4 < y$

In region (a) we used formula 7.12(21 of Ref. [43].

$$K_r(y) = \int_0^{\infty} \text{Cosh}(rt)\exp[-y\ \text{Cosh}(t)]dt$$

which can be written

$$K_r(y) = \int_0^{t_0} \text{Cosh}(rt)\exp[-y\ \text{Cosh}(t)]dt + R(r,t_0)$$

Using

$$\text{Cosh}(t) = \frac{1}{2}(e^t + e^{-t}) > \frac{1}{2}e^t$$

we get

$$R(r,t_0) \leq \frac{1}{2} \int_{t_0}^{\infty} (e^{rt} + e^{-rt}) \exp(-\frac{ye^t}{2}) dt$$

Taking

$$x = e^t, \quad x_0 = e^{t_0}, \quad \frac{dx}{x} = dt \quad \text{and} \quad x_0 > 1,$$

we get

$$R(r,x_0) \leq \frac{1}{2} \int_{x_0}^{\infty} (x^{r-1} + x^{(r-1)}) e^{-xy/2} dx$$

<u>for r = 4/3</u>; r-1 = 1/3 and -(r+1) = -7/3.

Therefore

$$R(4/3,x_0) \leq \frac{1}{2} \int_{x_0}^{\infty} (x+1) e^{-xy/2} dx$$

$$= \frac{1}{2}[\frac{2}{y}(x_0 2/y) e^{-x_0 y/2} + \frac{2}{y} e^{-x_0 y/2}],$$

or

$$R(4/3,x_0) \leq \frac{e^{-x_0 y/2}}{y}(x_0 + 1 + 2/y)$$

<u>for r = 1/3</u>; r-1 = -2/3 and -(r+1) = -4/3,

Therefore

$$R(1/3,x_0) \leq \frac{1}{2}\int_{x_0}^{\infty} e^{-xy/2}dx = \frac{e^{-x_0 y/2}}{y}$$

Since in Eq. (B-6)

$$y_b \geq y_0,$$

and we calculate $f(y_0,\theta)$ only for $y_0 \geq .1$, setting $R(r,x_0) \leq 10^{-7}$ gives

$$x_0 \tilde{<} 450 \quad \text{for} \quad r = 4/3, \text{ and}$$

$$x_0 \tilde{<} 400 \quad \text{for} \quad r = 1/3.$$

Thus, we conclude that

$$K_r(y) = \int_0^6 \text{Cosh}(rt)\exp[-y\ \text{Cosh}(t)]dt \qquad \text{(B-8)}$$

$$+ R(r,6)$$

where

$$R(r,t) \leq 10^{-7} \quad \text{for} \quad r = 4/3 \text{ or } 1/3, \text{ and } y \geq .1.$$

We calculate $K_r(y)$ for $.1 \leq y \leq 4$ by integrating Eq. (B-8) numerically in steps of $\Delta t = 10^{-3}$. For $y > 4$, we use formula 7.13(7) of Ref. [43]

$$K_r(h) = (\pi/2y)^{1/2}e^{-y}\left[\sum_{m=0}^{N-1} \frac{\Gamma(r+m+1/2)}{m!\,\Gamma(r+1/2-m)}(2y)^{-m} + 0(y^{-N})\right] \qquad \text{(B-9)}$$

We take N = 10, and therefore for $y > 4$, the order of the absolute error is less than

$$(\pi/8)^{1/2} e^{-4} 4^{-10} \sim 10^{-8}$$

6) For $y_a$ or $y_b$ which are greater than 30, we use the approximation

$$\int_{y_0}^{y_a, y_b} g(y)\,dy \cong \int_{y_0}^{30} g(y)\,dy \qquad \text{(B-10)}$$

For $y_1 > 30$ we can write

$$\int_{y_0}^{y_1} g(y)\,dy = \int_{y_0}^{30} g(y)\,dy + R(y_1),$$

where

$$R(y_1) = \int_{30}^{y_1} \mathrm{Sec}^{-1}(y/y_0)\, y^{4/3} K_{1/3}(y)\,dy$$

$$\leq (\pi/2) \int_{30}^{y_1} y^{4/3} K_{1/3}(y)\,dy$$

$$= (\pi/2)\left[-y^{4/3} K_{4/3}(y)\right]_{30}^{y_1}.$$

For $y \geq 30$, $y^{4/3} K_{4/3}(y)$ is a decreasing function.

Thus

$$R(y_1) \leq (\pi/2)(y_1 - 30)30^{4/3}K_{4/3}(30).$$

Taking $30 \leq y_1 \leq 10^4$,

$$R(30 \leq y_1 \leq 10^4) \leq (\pi/2)^{3/2}10^4 30^{5/6}e^{-30} \sim 10^{-7}$$

7) The numerical integration of $\int g(y)dy$ is done in steps of $\Delta y = .01$.
Additional information concerning the numerical integration can be learnt from the program itself.

The Program

```
C    F(YO,TETA)   CALCULATION
C
C
C    SET CONSTANTS
C
       PI=3.14159265
       PI2=PI/2.
       A=1.586820/2.
       B=1.125040
       DYO=.1
       XR=62.
       DG=.01
       WRITE(6,72)
   72 FORMAT(2X,' YO',6X,'TETA',10X,'YB',12X,'FIRST TERM',4X,'YBK(YB)',7X
     C,'SECOND TERM',3X,'INTG(YA,YO)',3X,'INTG(YB,YO)',3X,'SUM IN PAR',4
      CX,'F(TETA)'//2X,130(1H=)//)
C
C    CALCULATE YO,YB,TETA
C
       DO 101 I=1,300
       XI=FLOAT(I)
       YO=XI*DYO
       Z=YO/XR
       TET=ARSIN(Z)
       TETA=TET/2.
       YB=YO/COS(TETA)
C
C    CALCULATE FIRST TERM
C
       TERF=(PI2-TETA)*B
C
C    CALCULATE SECOND TERM
C
C    CALCULATE  KSUB(4/3)
C
       XN=4./3.
       BL=BSL(XN,YB)
       TERS1=BL*(YB**XN)
       TERS=TETA*TERS1
C
C    CALCULATE THIRD AND FORTH TERMS
C
```

```
      XIA=0.
      XIB=0.
      X=1./3.
C
C    G(YO)=0. BECAUSE INVSEC(YO/YO)=0
C    INVSEC(Y/YO)=ARCOS(YO/Y)
C
      Y=30.
      Z=YO/Y
      XSC=ARCOS(Z)
      BL=BSL(X,Y)
      XS=XSC*(Y**XN)*BL/2.
      XIA=XIA+XS
      Y=YB
      BL=BSL(X,Y)
      XS=TETA*(Y**XN)*BL/2.
      XIB=XIB+XS
      XM=(30.-YO)/DG
      M=IFIX(XM)
      DO 102 J=1,M
      XJ=FLOAT(J)
      Y=YO+DG*XJ
      Z=YO/Y
      XSC=ARCOS(Z)
      BL=BSL(X,Y)
      XS=XSC*BL*(Y**XN)
      XIA=XIA+XS
      IF(Y.GT.YB) GO TO 7
      XIB=XIB+XS
    7 CONTINUE
  102 CONTINUE
      TERT=XIA*DG
      Z1=YB-YO
      DE=DG
C
C    FOR DG=.01
C
      IF(Y.LE.27.)  DE=Z1
C
      TERFO=XIB*DE
      FT=TERF-TERS-TERT-TERFO
      FTETA=FT*A/YO
      WRITE(6,71)  YO,TETA,YB,TERF,TERS1,TERS,TERT,TERFO,FT,FTETA
   71 FORMAT(2X,F4.1,9(2X,F12.8))
  101 CONTINUE
      STOP
      END
```

```
      FUNCTION BSL(R,S)
C
C     R=NU,S=Y,BSL=KNU(Y)  MODIFIED BESSEL FUNCTION OF THE THIRD KIND
C
C
      IF(S.GE.4.0) GOTO 1
C
C
C     K(Y)  FOR .1<S<4.
C     CALCULATE BY USE OF EQUATION 7.12(21) OF REF.(43) VOL 2
C     THE INTEGRATION IS CARRIED IN STEPS OF DELTA T=.001 (ERROR DUE TO NU
C     MERICAL INTEGRATION IS <10-6)
C     THE INTEGRATION IS TRUNCATED AT T=6.0 .ERROR DUE TO TRUNCATION <10-7
      CUT=-100.
      DELTA=.001
      M=6000
      M1=M+1
      BK=0.
      DO 103 K=1,M1
      K1=K-1
      XKA=FLOAT(K1)
      T=XKA*DELTA
      TN=T*R
      AC=COSH(T)
      BC=COSH(TN)
      CC=(-1.)*AC*S
      C1=CC+ALOG(BC)
      IF(C1.LT.CUT) GO TO 9
      XG=EXP(C1)
      GO TO 28
    9 XG=0.0
   28 CONTINUE
      IF(K.EQ.1.OR.K.EQ.M1) XG=XG/2.
      BK=BK+XG
  103 CONTINUE
      BSL=BK*DELTA
      GO TO 8
    1 CONTINUE
```

```
C
CC
C     K(Y)  FOR  S>4.
C     REF(43)  7.13(7)
C     UP TO (INCL) 10TH TERM
C     RELATIVE ERROR <10-6
CC
C
      PI=3.14159265
      PI2=PI/2.
      AX=.5+R
      AZ=1.
      AS=1.
      DO 104 I=1,9
      XI=FLOAT(I)
      AS=AS*(AX-1.+XI)*(AX-XI)/(2.*S*XI)
      AZ=AZ+AS
  104 CONTINUE
      SM=S*(-1.)
      BSL=((PI2/S)**.5)*(EXP(SM))*AZ
    8 CONTINUE
      RETURN
      END
```

## LIST OF REFERENCES


1. Tatarski, V.I., Wave Propagation in a Turbulent Medium, McGraw-Hill, 1958.

2. Tatarski, V.I., The Effects of the Turbulent Atmosphere on Wave Propagation, Translated from Russian by the Israel Program for Scientific Translations, Jerusalem 1971, Published by the National Science Foundation, Washington, D.C., 1971.

3. Fried, D.L., "Propagation of a Spherical Wave in a Turbulent Medium", JOSA, Vol. 57, p. 175, 1967.

4. Lutomirski, R.F., and Yura, H.T., "Propagation of a Finite Optical Beam in an Inhomogeneous Medium", Appl. Opt., Vol. 10, P. 1652, 1971.

5. Ishimaru, A., Wave Propagation and Scattering in Random Medium, Academic Press, 1978.

6. Lee, R.W., and Harp, J.C., "Weak Scattering in Random Media, with Applications to Remote Probing", IEEE Proc., Vol. 57, P. 375, 1969.

7. Clifford, S.F., Ochs, G.R., Lawrence, R.S., "Saturation of Optical Scintillation by Strong Turbulence", JOSA, Vol. 64, P. 148, 1974.

8. Fante, R.L., "Electromagnetic Beam Propagation in Turbulent Media", IEEE Proc., Vol. 63, P. 1669, 1975.

9. Fante, R.L., "Electromagnetic Beam Propagation in Turbulent Media; An Update", IEEE Proc., Vol. 68, P. 1424, 1980.

10. Dashen, R., "Path Integrals for Waves in Random Media", J. Math. Phys., Vol. 20, P. 894, 1979.

11. Strohbehn, J.W., Clifford, S.F., "Polarization and Angle of Arrival Fluctuations for Plane Wave Propagated Through a Turbulent Medium", IEEE Trans., Vol. AP-15, P. 516, 1967.

12. Collett, E., Alferness, R., "Depolarization of a Laser Beam in a Turbulent Medium", JOSA, Vol. 62, P. 529, 1972.

13. Hohn, D.H., "Depolarization of a Laser Beam at 6328 Å Due to Atmospheric Transmission", Appl. Opt., Vol. 8, P. 367, 1969.

14. Hill, R.J., Clifford, S.F., Lawrence, R.S., "Refractive-index and Absorption Fluctuations in the Infrared Caused by Temperature, Humidity, and Pressure Fluctuations", JOSA, Vol. 70, P. 1192, 1980.

15. Hufnagel, R.E., "Optical Propagation Study", Tech. Rep. No. RADC-TR-65-511, January 1966.

16. Lumley, J.L., Panofsky, H.A., The Structure of Atmospheric Turbulence, John Wiley, 1964.

17. Kolmogorov, A.N., "A Refinement of Previous Hypotheses Concerning the Local Structure of Turbulence in a Viscous Incompressible Fluid at High Reynolds Number", J. Fluid Mech., Vol. 13, P. 82, 1962.

18. Oboukhov, A.M., "Some Specific Features of Atmospheric Turbulence", J. Fluid Mech., Vol. 13, P. 77, 1962.

19. Yura, H.T., "Optical Beam Spread in a Turbulent Medium; Effect of the Outer Scale of Turbulence", JOSA, Vol. 63, P. 107, 1973.

20. Hill, R.J., Clifford, S.F., "Modified Spectrum of Atmospheric Temperature Fluctuations and its Application to Optical Propagation", JOSA, Vol. 68, P. 892, 1978.

21. Feynman, R.F., Hibbs, A.R., Quantum Mechanics and Path Integrals, McGraw-Hill, 1965.

22. Palmer, D.L., "An Introduction to the Applications of Feynman Path Integrals to Sound Propagation in the Ocean", NRL Rep., 8148, January 1978.

23. Yura, H.T., "Physical Model for Strong Optical Amplitude Fluctuations in a Turbulent Medium", JOSA, Vol. 64, P. 59, 1974.

24. Phillips, R.L., Andrews, L.C., "Laser Weapon Fire Simulation of a Long Range Gunnery Training; A Universal Math. Model and Experimental Verification", Rep. No. 80-81-2, December 1980.

25. Parry, G., Pusey, P.N., "K Distribution in Atmospheric Propagation of Laser Light", JOSA, Vol. 69, P. 796, 1979.

26. Clifford, S.F., Hill, R.J., "Relation between Irradiance and Log-Amplitude Variance for Optical Scintillation Described by the K Distribution", JOSA, Vol. 71, P. 112, 1981.

27. Fante, R.L., "Intensity Scintillation of an EM Wave in Extremely Strong Turbulence", IEEE Trans., Vol. AP-25, P. 266, 1977.

28. Yura, H.T., "Signal to Noise Ratio of Hetrodyne Lidar Systems in the Presence of Atmospheric Turbulence", Optica Acta, Vol. 26, P. 627, 1979.

29. Bensimon, D., Englander, A., Strikman, S., Slatkine, M., Treves, D., "Statistical Properties of the He-Ne Laser Radiation Reflected through a Turbulent Atmosphere", Appl. Opt., Vol. 20, P. 947, 1981.

30. Lutomirski, R.F., Warren, R.E., "Atmospheric Distortion in a Retroreflected Laser Signal", Appl. Opt., Vol. 14, P. 840, 1975.

31. Hansen, J.P., Madhu, S., "Angle Scintillations in the Laser Return from a Retroreflector", Appl. Opt., Vol. 11, P. 233, 1972.

32. Greenwood, D.P., "Tracking Turbulence Induced Tilt Errors with Shared and Adjacent Apertures", JOSA, Vol. 67, P. 282, 1977.

33. Lee, M.H., "Variance and Covariance of Irradiance of a Finite Beam in Extremely Strong Turbulence", JOSA, Vol. 68, P. 167, 1978.

34. Fried, D.L., "Statistics of Geometric Representation of Wavefront Distortion", JOSA, Vol. 55, P. 1427, 1965.

35. Bateman Manuscript Project, Tables of Integral Transforms, Ed: Erdelyi, A., California Institute of Technology, McGraw-Hill, 1954.

36. Smith, J., Pries, T.H., "Temporal-Frequency Spectra for Waves Propagating over Straight and Folded Paths; A Comparison", Appl. Opt., Vol. 14, P. 1161, 1975.

37. Smith, J., "Folded Path Weighting Function for a High Frequency Spherical Wave", JOSA, Vol. 63, P. 1095, 1973.

38. Gamo, H., Jagannathan, N., Majumdar, A.K., "A Comparison of a Corner-Cube Reflector and a Plane Mirror in Folded-Path and Direct Transmission through Atmospheric Turbulence", SPIE, Vol. 125, P. 30, 1977.

39. Fried, D.L., "Reconciliation of Results in Aperture Averaging of Scintillation", Rep. No. TR-118, October 1973.

40. Young, A.T., "Aperture Filtering and Saturation of Scintillation", JOSA, Vol. 60, P. 248, 1970.

41. Crittenden, E.C. Jr., Cooper, A.W., Milne, E.A., Rodeback, G.W., Armstead, R.L., Kalmback, S.H., Land, D., Katz, B., "Optical Resolution in the Turbulent Atmosphere of the Marine Boundary Layer", Rep. No. NPS 61-78-003, February 1978.

42. Hodgini, T.J., Optical Scintillation Measurements for Single and Folded Paths, Master's Thesis, Naval Post-graduate School, 1982.

43. Bateman Manuscript Project, Higher Transcendental Functions, Ed: Erdelyi, A., California Institute of Technology, McGraw-Hill, 1954.

44. Lutomirski, R.F., Huscke, R.E., Meecham, W.C., Yura, H.T., "Degradation of Laser Systems by Atmospheric Turbulence", R-1171-ARPA/RC, June 1973.

## INITIAL DISTRIBUTION LIST

| | | No. Copies |
|---|---|---|
| 1. | Defense Technical Information Center<br>Cameron Station<br>Alexandria, Virginia 22314 | 2 |
| 2. | Library, Code 0142<br>Naval Postgraduate School<br>Monterey, California 93940 | 2 |
| 3. | Department Chairman, Code 61Dy<br>Department of Physics and Chemistry<br>Naval Postgraduate School<br>Monterey, California 93940 | 1 |
| 4. | Professor E.C. Crittenden, Jr. Code 61Ct<br>Naval Postgraduate School<br>Monterey, California 93940 | 8 |
| 5. | Professor F.R. Buskirk, Code 61Bs<br>Naval Postgraduate School<br>Monterey, California 93940 | 1 |
| 6. | Professor D.J. Collins, Code 67Co<br>Naval Postgraduate School<br>Monterey, California 93940 | 1 |
| 7. | Professor A.W. Cooper, Code 61Cr<br>Naval Postgraduate School<br>Monterey, California 93940 | 1 |
| 8. | Professor G.E. Latta, Code 53Lz<br>Naval Postgraduate School<br>Monterey, California | 1 |
| 9. | Professor E.A. Milne, Code 61Mn<br>Naval Postgraduate School<br>Monterey, California 93940 | 1 |
| 10. | Professor G.W. Rodeback, Code 61Rk<br>Naval Postgraduate School<br>Monterey, California 93940 | 1 |
| 11. | Professor S. Yatziv<br>Rachach Institute<br>The Hebrew University<br>Jerusalem, ISRAEL | 1 |

12. Professor S. Strikman 1
Weizman Institute
Rehovot, ISRAEL

13. Professor L.C. Andrews 1
Department of Mathematics and Statistics
University of Central Florida
Orlando, Florida 32816

14. Commander 1
Waterways Experimental Station
ATTN: CPT T.J. Hodgini
Vicksburg, Mississippi 39180

15. A. Ze'evi 7
2 Hatamar Street
Petuch-Tikva, 49212
ISRAEL

Thesis
Z314
c.1
198185
Ze'evi
Optical scintillation on folden paths.